Brownian Dynamics Simulations of DNA Complexation with Nano-Cationic Dendrimers

استخدام محاكاة الحركة البراونية لدراسة تفاعل المادة الوراثية (DNA) مع مركبات النانو كاتيونيك ديندريمرز

Doa Hawamdeh

Thesis committee:

Dr. Abdallah Sayyed-Ahmad (Principal advisor)

Dr. Khawlah Qamheih (Member)

Dr. Wafaa Khater (Member)

This thesis was submitted in partial fulfillment of the requirements for the degree of Master of Physics from the Faculty of Graduate Studies at Birzeit University, Palestine.

January 2018

Brownian Dynamics Simulations of DNA Complexation with Nano-Cationic Dendrimers

استخدام محاكاة الحركة البراونية لدراسة تفاعل المادة الوراثية (DNA) مع مركبات النانو كاتيونيك ديندريمرز

Doa Hawamdeh

Accepted by the Faculty of Graduate Studies, Birzeit University, in

partial fulfillment of the requirements of degree of Master of Physics.

Thesis committee:

Abdallah Sayyed-Ahmad, Ph.D. (Principal Advisor)

Khawlah Qamheih, Ph.D. (Member)
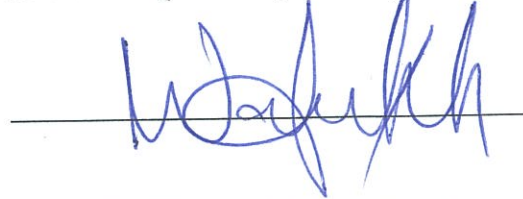
Wafaa Khater, Ph.D. (Member)

January 2018

ACKNOWLEDGEMENT

I would like to express my sincere appreciation to my advisor Dr. Abdallah Sayyed-Ahmad for his continuous support, patience, motivation, immense knowledge and guidance that helped accomplishing this study. I could not have imagined having a better advisor and mentor during my Master's study. I would also like to thank my thesis committee: Dr. Khawlah Qamheih and Dr. Wafa' Khater for their encouragement, insightful comments and the interesting questions which inspired me to widen my research from various perspectives. Finally, I would like to extend special thanks for my family for their support and encouragement.

ABSTRACT

Gene therapy holds a promise in treating genetic diseases by directly delivering therapeutic DNA into living cells. Although viruses have been shown to be efficient delivery vectors, their toxicity has limited their general use. As an alternative, polyamidoamine (PAMAM) dendrimers are considered to be ideal candidates for synthetic vectors due to their unique intrinsic biophysical properties. At neutral pH, a PAMAM dendrimer is cationic and can effectively bind to negatively charged nucleic acid strands to form efficient transfection complexes.

In this work, we carried out multiple Brownian dynamics simulations to investigate the physicochemical properties of DNA-PAMAM dendrimers complexes for different lengths of single- and double- stranded DNA complexed with various generations of PAMAM dendrimer. PAMAM dendrimer is represented by a positively charged sphere whereas a bead-spring model is used to model DNA strands. Our results indicate that the formation of DNA-dendrimer complexes is affected by the salt concentration. At low salt concentration (10-100mM) a DNA chain wraps strongly around the dendrimer, whereas the stronger electrostatics screening effects at high salt concentration limit the wrapping of DNA chain around dendrimers. Furthermore, the morphologies of the aggregates depend on the interaction between DNA and PAMAM dendrimer as well as the PAMAM generation number. For example, G2 with dsDNA seems to have a rod-like structure while ssDNA with G4 trends to give a piece of toroid. Also the flexible dsDNA can form toroidal morphologies with G2 dendrimers while the aggregates of G2 dendrimers and the stiff dsDNA have rod-like structure.

ملخص

يلعب العلاج الجيني دورا مهما في علاج الأمراض الوراثية عن طريق نقل المادة الوراثية (DNA) إلى داخل الخلية الحية. بالرغم من توظيف الفيروسات كناقل حيوي فعال للمادة الوراثية إلا أن سميتها العالية قللت من استخدامها. تعتبر المركبات الكيميائية الصناعية (PAMAM dendrimers) بديلا مثاليا لبناء نواقل للمادة الوراثية بسبب صفاتها البيو فيزيائية الفريدة. حيث أنها موجبة الشحنة على درجة حموضة متعادلة مما يمكنها من التجاذب مع النيوكليوتيدات سالبة الشحنة لتشكل مركبات ناقلة عالية الفعالية.

في هذا البحث استخدمنا محاكاة الحركة البراونية لدراسة الخصائص الفيزيائية للمركبات الناتجة من التفاعل الكهربائي بين أجيال مختلفة من الديندريمرز و (ssDNA ,dsDNA), حيث استخدمت كرة موجبة الشحنة لتمثيل الدينريمرز. في حين مثلنا (DNA) باستخدام نموذج الخرزة والنابض. وجدنا أن تشكل مركب من ال DNAو الديندريمرز يتأثر بتركيز الأملاح الموجودة في الماء. حيث أنه على تركيز منخفض يتمكن ال DNAمن الالتفاف بشكل قوي حول الديندريمر, وكلما زاد تركيز الأملاح يضعف التجاذب الكهربائي بين DNA و الديندريمرز. بالمقارنة مع النتائج التجريبية وجدنا أن الجيل الثاني من الديندريمرز عندما يلف DNA حوله يظهر بشكل يشبه العصا. في حين أن الجيل الرابع يعطي شكلا حلقيا لولبيا (toroidal structure) مع ssDNA.

TABLE OF CONTENTS

LIST OF FIGURES

LIST OF TABLES

Chapter 1: INTRODUCTION

1.1. Structure and Function of DNA

Deoxyribonucleic acid (DNA) is a molecule that serves as carrier of genetic information and consequently plays an important role in the growth, development, functioning and reproduction of living cells. Its structure was first characterized in 1953 by James Waston and Francis Crick[2]. In living cells, DNA molecules organize in two biopolymer strands coiled around each other to form a double helix. These strands are called polynucleotides since they are composed of simpler monomer units called nucleotides (see Figure 1.1).
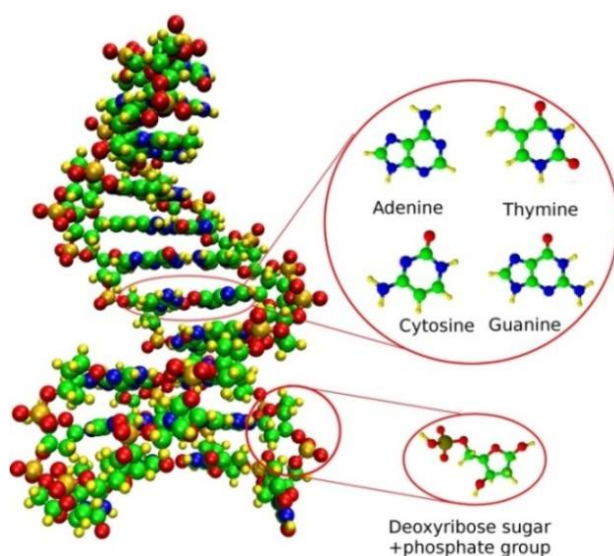
Figure 1.1: A CPK representation of all atom structure of double helix DNA. Nitrogen, oxygen, carbon, hydrogen and phosphorus are shown in blue, red, green, yellow and orange, respectively. DNA is a polymer of nucleic acids, each nucleic acid is composed of nitrogen bases (adenine, thymine, guanine and cytosine), deoxyribose sugar and phosphate group. The structure is obtained from www.pdb.org.

Each nucleotide is composed of one of four hydrophobic nitrogen bases (cytosine (C), guanine (G), adenine (A) or thymine (T)), a phosphoric acid group

and a deoxyribose sugar. Phosphate groups give DNA its overall negative charge. The sugar of one nucleotide is linked covalently to the phosphate group of the next nucleotide, resulting in alternating sugar-phosphate backbone. The nitrogen bases of the two separate strands are then joined together by hydrogen bonds to make a double stranded DNA.[2-4]

A crucial property of DNA is that it can replicate. Each strand of DNA in the double helix can serve as a template for duplicating the sequence of its nucleotide bases. This is critical for passing biological information when cells divide because each new cell needs to have an exact copy of the DNA present in its parent cell.[4] DNA forms genes which are the basic physical and functional unit of heredity. Genes act as instructions to make molecules called proteins[5]. In humans, the whole genome is comprised of three billion base pairs (bp), two copies of which make up two meters of DNA chains that have to be contained within the micron-sized nucleus of each cell.[6] In eukaryotic cell nucleus DNA is wrapped around a positively charged protein known as histone and forms the nucleosome structure[7]. These nucleosomes are further folded into higher order structures called chromosomes. [6, 8, 9]

1.2.   Gene Therapy as a Mean for Treating Genetic Diseases

Genetic abnormalities often lead to dangerous diseases that adversely affect human health all around the world[10]. Examples of these diseases include autism, hemophilia, Parkinson and cancers. Genetic abnormalities can be as small as a single-base mutation in just one gene, or they can involve the addition or subtraction of entire chromosomes[11]. Single-base disorders involve mutations in the DNA sequences of single genes, so the protein that the gene codes is either

2

altered or missing, like Andenosine deaminase (ADA) deficiency disease which is caused by a mutation on chromosome 20 which includes the gene coding for the enzyme adenosine deaminase (ADA). ADA is responsible for breaking down a toxic substance called deoxyadenosine that can destroy infection-fighting T and B lymphocytes[12-14] . On the other hand, in the chromosomal abnormalities, entire chromosomes or large segments of them can be missing (e.g. Turner syndrome), duplicated (e.g. Down syndrome) or otherwise altered (e.g. Alzheimer's disease). For example, Alzheimer's is a disease that affects the parts of the brain that are important for memory, thought and language. The most common form of the disease is caused by a mutation on the apolipoprotein E (apoE) gene on chromosome 19[15].

Studying the complexation of biomolecules plays an important role in understanding diseases and development of new therapeutics[16-20]. Therefore treating genetic diseases can be achieved by the delivery of a therapeutic agent to human cells at the site of its action to regulate targeted gene expression in a process called gene therapy[21-23]. Gene therapy is still mostly an experimental technique that target genes to treat or prevent diseases by replacing a mutated gene that causes disease with a healthy copy of the gene, inactivating a mutated gene that is working improperly, or introducing a new gene into the body to help fight a disease[24, 25]. In the future, this technique may allow doctors to treat a disorder by inserting a gene into a patient's cells instead of using drugs or surgery[26].

Although gene therapy is a promising treatment option for a number of diseases (including inherited disorders, some types of cancer, and certain viral infections), the technique remains risky and is still under intensive study to make

3

sure that it will be safe and effective[27]. Gene therapy is currently only being tested for the treatment of diseases that have no other alternative cures. The success of gene therapy depends mainly on the development of a vector or vehicle that can selectively and efficiently transport a gene to target cells with minimal toxicity[10, 28]. Since all of the genetic information is carried on the DNA, the challenge is to find an effective vector to condense the therapeutic DNA to transport it into the cell nucleus. Condensation of DNA protects it against degradation and helps transporting it across membranes which is a major barrier towards gene therapy [3, 27]. Although viruses have been demonstrated to be efficient delivery vectors[29], their toxicity and immunogenicity have limited their general use[10, 30]. As an alternative, many synthetic compounds are developed for the potential use as non-viral gene delivery vehicles such as varying generation dendrimers[10, 24, 31].

1.3. PAMAM Dendrimers

Dendrimers which have been discovered in 1980s are considered as an appropriate candidate for synthetic vectors due to their unique intrinsic properties[30]. They are radially symmetric complex molecules that have a homogenous and monodisperse chemical structure. They mainly consist of hydrogen, nitrogen, oxygen and carbon[32-35] and are characterized by highly branched 3D structure in their outer most dendritic shell[36]. The name arises from 'dendron' which means tree in Greek[37-39]. Dendrimers have an initiator core, branching units called dendrons and terminating units[40-43]. In general, the core of a dendrimer may have any number of branches but typical dendrimers have between two and four branches on the core [34].

4

Dendrimer is specified by its generation which is determined by the number of branching points from its core to the surface groups. The core is called the *0th* generation (G_0), and each successive addition of branching points is denoted as G_n, with n denoting the generation number[34, 37, 44, 45]. Figure 1.2 is a schematic diagram that illustrates the structure of a dendrimer. Its size increases for each successive generation by approximately 1 nm in diameter. For example, generation zero starts from a diameter of 1.5 nm generation 10 may reach a diameter of 13.5 nm [46].
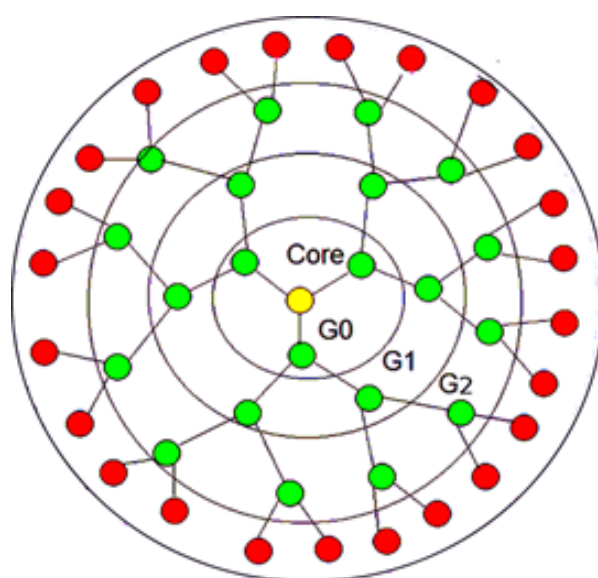
Figure 1.2: Schematic diagram of a dendrimer structure. A dendrimer is composed of an initiator core (yellow), branching units (green) and terminal units (red).

The two most commonly used and commercially available dendrimers are the poly-amidoamine (PAMAM) dendrimers (see for example Figure 1.3) and the poly-propylene imine (PPI)[47] dendrimers. The core of PAMAM dendrimer is ethylene-diamene, which allows for four polyamidoamine branching units to be placed on it for the construction of the zero generation dendrimer.
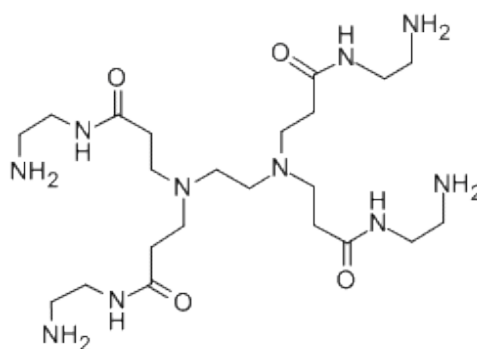
Figure 1.3: Chemical structure of G_1 PAMAM dendrimer.

The size and complexity of a PAMAM dendrimer increase with its generation number. As a demonstration, Figure 1.4 depicts the complexity of an all atom structure of G6 PAMAM dendrimer. A benzene ring on the other hand forms the core of the PPI dendrimers and it is connecting to phenyl-acetylene branching arms[10, 38]. Other commonly used dendrimers include poly(ester)[48], triazines[49], and phosphorous[50] containing dendrimers. The end groups can be further modified with other chemical moieties including folate, RGD, glutathione, immunoglobulins(Ig), lipids and bio-responsive elements or polymers e.g., polyethyleneglycol (PEG) to optimize dendrimer biological properties[51-53].
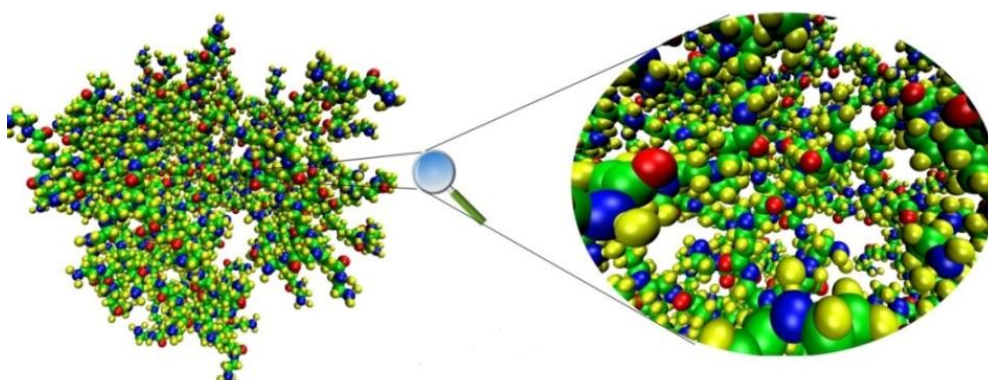
Figure 1.4: All atom structure of generation 6 PAMAM dendrimer shows the hollow cavities inside the dendrimer. Blue, red, green, yellow are for nitrogen, oxygen, carbon, and hydrogen respectively.

6

There is a significant uncertainty about the detailed structure and stability of high generation dendrimers. Theoretical calculations on PAMAM dendrimers by Gennes and Harvet [54] showed that the growth of dendrimer is limited because the surface becomes too crowded preventing further growth. Whereas, computational studies by Goddard and Tomalia[55] indicated that above the fourth generation, the dendrimer structure has hollow cavities inside[56].

Dendrimers grow through a variety of chemical reactions, they are constructed using either a divergent approach or a convergent one[33, 38, 57]. In the divergent methods which was pioneered by Newkome and Tomalia[37, 56], the structure is initiated from the core of the dendrimer to which branches are added in a step-wise fashion, as each layer is added a generation is completed. The process is repeated for consequent generations until a dendrimer is grown layer after layer. This technique is good for generating large quantities of dendrimers. Unfortunately, serious difficulties appear due to the presence of side reactions with the end groups. As a result, the convergent method is developed in which a dendrimer is similarly built stepwise, starting from the end groups and continuing inwards, while the polymer branches are attached to the core. The convergent methods are the preferred technique for the synthesis of dendrimers but they are not used for constructing high generations because steric problems arise in the reactions of dendrons and the core molecule[58].

The physicochemical properties of dendrimers such as the high degree of branching, water solubility, uniform size, well defined molecular weight and availability of internal cavities make them ideal for DNA-delivery in gene therapy applications and drug delivery systems[35, 36, 54, 59-62]. As the dendrimer generation

7

increases, the branches arrange themselves in the form of a sphere around the core with most of space remains hollow all the way towards core. This hollow region can be used for drug entrapment. The advantage of dendrimers is that they can be synthesized and designed for specific applications. The outer surface of dendrimers has multiple functional groups, which can be selectively modified to attach vector devices for targeting a particular site in the body [31, 57, 63-65].

1.4. Dendrimer-DNA Complexation

Dendrimers may also have functional groups attached to their end groups that enable them to target specific tissues and be selectively in their endocytosis. This means that a dendrimer could potentially be used to selectively deliver toxins to cancer cells while preserving healthy tissue cells[57, 66]. In addition to drug delivery, dendrimers also have potential applications in solar energy conversion. Organic photovoltaic devices using dendrimers could provide another path to bulk silicon photovoltaic devices which can improve the efficiency and cost of solar cells[67, 68].
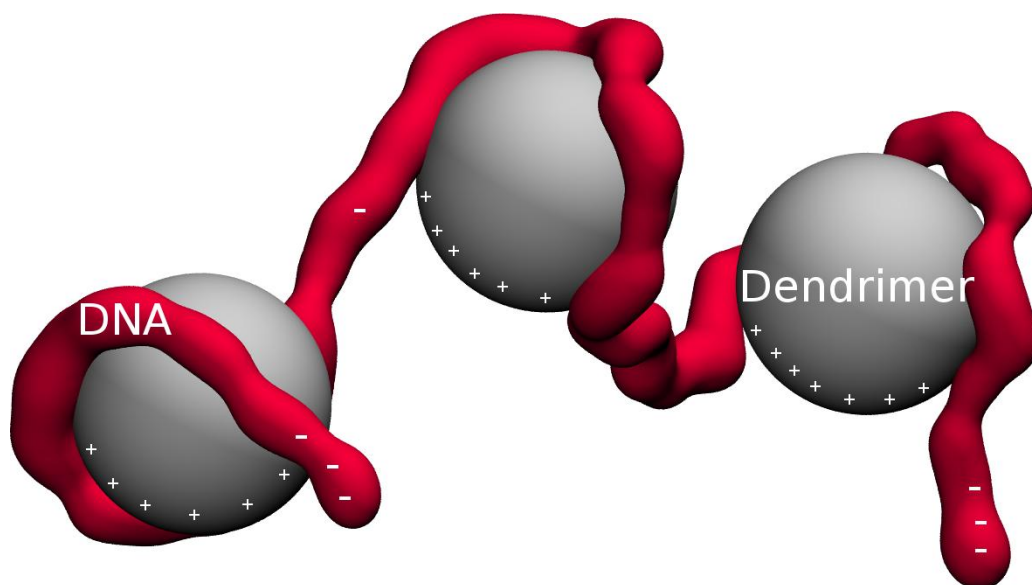
Figure 1.5: An example of DNA-dendrimer binding: the electrostatic interactions between negative DNA chain and positive dendrimer allow the DNA to wrap around the positive dendrimer to form a complex.

At neutral physiological pH a PAMAM dendrimer is highly positively charged and can effectively bind to negatively charged DNA to form a lower toxicity and transfection efficient complexes (see Figure 1.5) that can be used as a gene delivery vector inside mammalian cells[43, 69, 70]. Complexes of dendrimers with DNA molecules in any solvent are stabilized by electrostatic forces. The properties of these complexes were studied by various experimental, computational and theoretical methods. DNA condensation using PAMAM dendrimer was first reported in a study using agarose gel electrophoresis.[71] Many experimental approaches such as electron paramagnetic resonance (EPR)[72], small angle neutron scattering (SANS),[73, 74] X-ray,[75, 76] nuclear magnetic resonance (NMR)[77], dynamic light scattering[78, 79] and fluorescence resonance energy transfer (FRET) are used to study the structure and the effective interaction of dendrimer with other molecules.[10] Also Fourier transform infrared spectroscopy (FTIR), UV-visible, and circular dichroism (CD) spectroscopic methods and atomic force microscopy (AFM), were used to analyze the macromolecule binding mode, the binding constant, and the effect of dendrimer complexation on DNA stability, aggregation, condensation and conformation.[3, 80]

Computer simulations at different levels of complexity are also commonly used to achieve a quantitative understanding of DNA-dendrimer complexation. For example, atomistic molecular dynamics (MD) simulations of DNA-dendrimer complexes have provided atomic-scale insights into their structure and dynamics. However, due to the large system size and time scale limitations, atomistic models are currently limited to studying low generation dendrimers complexation with small DNA strands. Simulations of long DNA strands with higher order dendrimer generations such as G7 and G8 are not routinely possible. To overcome

9

these limitations, several coarse grained (CG) models have been proposed. In the coarse-grained molecular dynamics simulations, a group of atoms are mapped to a single interaction site. This method enables the simulation of larger systems for longer time scales than that is possible by all-atom molecular dynamics simulations[81, 82]

A large number of simulation studies of the complexation of dendrimer with DNA and other polyelectrolytes have been reported in the literature. The most notable ones are the following: Welch and Muthukumar used Monto Carlo(MC) simulations to study the complexation between a model dendrimer (chemically closer to Poly-Propyl-Imine(PPI) dendrimer) and charged linear chains under varying pH conditions.[83] While, Lyulin *et.al*, have reported the structural aspects of the complexes formed by charged dendrimer and oppositely charged linear polyelectrolyte(LPE) in dilute solution using Brownian Dynamics (BD) simulation and compared their results with results obtained using mean-field theory. In their work, dendrimers and an LPE chain are represented by a set of beads with a friction coefficient connected by rigid bonds, without taking into consideration any valence and torsion-angle potentials. They found that when the LPE and the dendrimer had the same charge, the LPE wrapped the dendrimer surface, leading to a decrease in the radius of gyration of the dendrimer. For longer LPE chains, more chain monomers were adsorbed on the dendrimer than was needed for dendrimer neutralization[84, 85]. In another study, the charge inversion of dendrimers in complexes with linear polyelectrolyte were obtained using the same model[86]. BD simulations were also employed by Lyulin's group to investigate the structural properties of complexes formed by two dendrimers with charged terminal groups and oppositely charged long linear polyelectrolyte[85].

Terao and Nakayama performed stochastic MD simulations to study the structure of charged dendrimers of various generations (G5, G6, and G7) at various pH values. They found that the radius of gyration strongly depends on the pH values. Furthermore, the pH dependence of the radius of gyration decreases at a higher generation number[87].

Maiti and Bagchi investigated the complexation of PAMAM dendrimers of generation (G2-G4) at various protonation levels and 38 base pair ssDNA in explicit water and the presence of counter-ions by performing atomistic MD simulation. In addition to studying the structural aspects of the complex at various pH conditions, they studied the effect of ssDNA sequence on DNA-PAMAM dendrimer complexation.[43] The effect of flexibility/rigidity of dendrimers on dendrimer-gene complexes was studied by Pavan and coworkers with all atom MD simulations. They studied the interactions between different PAMAM generations and siRNA. They revealed that G4 is able to adapt over the double strands in order to optimize the interactions, while G6 is almost insensitive to the presence of the charged siRNA. Also, they investigated the interactions between Newkome-type dendrons with nucleic acids and found that the binding affinity is very sensitive to salt concentration present in the solution. For example, at 150 mM NaCl concentration, DNA efficiently binds with generations larger than G2, because these generations gives enough surface ligands which can use some of them to protect DNA from destabilizing interaction with the charged ions in the external solutions.[88] Lyulin and co-workers also presented extensive MD simulations of complexes comprised of a coarse-grained charged model for a dendrimer of the 4th generation and a short polyelectrolyte chain of opposite charge with incorporation of counter-ions and explicit solvent molecules.[86, 89] In the work of Tian *et al*[90],

11

extensive coarse grained MD simulations were performed to explore the influence of rigidity of linear polyelectrolyte (LPE) on the dendrimer-LPE complexes. Qamhieh and coworkers studied analytically the DNA-dendrimer complexation using the modified Schiessel model for semi flexible PE chains of different lengths (680 nm and 1472.5 nm) and soft spheres represent G4 PAMAM dendrimer. They found that the optimal wrapping length for the shorter and longer DNA are 15.69 and 12.25 nm respectively [69, 91].

Shi Yu and Ronald Larson used the Monte Carlo simulations to study the effect of PAMAM dendrimer size and charge on its interactions with double-stranded DNA at different values of salt concentration. They found that the increasing of the salt concentration has the same effects on dendrimer generation as increasing pH, since at high pH small of the dendrimer terminal groups is protonated which weakens the attractions between the negative charges on the DNA and the positive charges on the dendrimer[92].

The term complex is used to represent the structure formed by one dendrimer and the part of a DNA molecule that wraps around it. Whereas, the
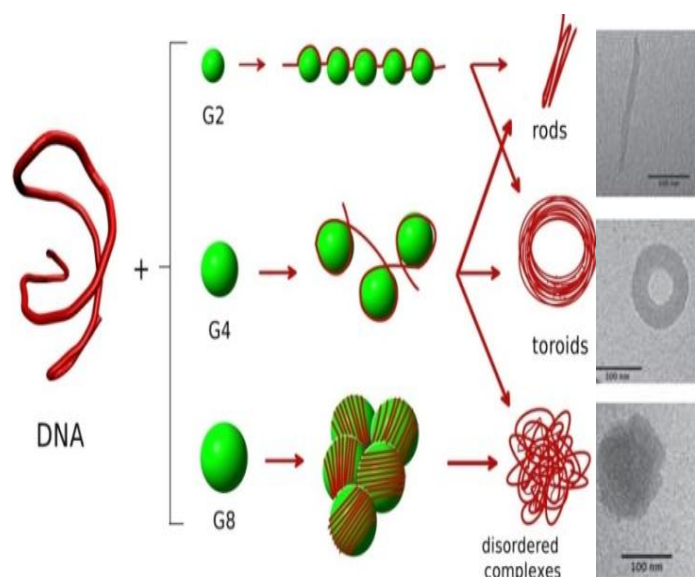
Figure 1.6: A schematic representation that illustrates the morphology of the complexes resulted from the wrapping of DNA around dendrimers of different generations[1].

structure formed between the entire DNA molecule and multiple dendrimers is termed an aggregate. Experimental studies of the complexes formed between linearized DNA plasmids and PAMAM dendrimers revealed that low generation dendrimers (G1 and G2) form higher order toroidal and rod-like structures, while high generation numbers (G6 and G8) form globular aggregates[93]. G4 serves as a border case as it can form globular as well as toroidal morphologies as illustrated in Figure 1.6[94]

In this study we used Brownian dynamics simulations to investigate the physicochemical properties of different DNA-PAMAM dendrimers complexes each of which is characterized by different lengths of single- and double-stranded DNA (ssDNA and dsDNA) along with various generations of PAMAM dendrimer. PAMAM dendrimer is represented by positively charged spheres whereas a bead-spring model is used to model the DNA stands. We also studied the effect of salt concentration on the complexation between ssDNA and dsDNA with different generations (G2, G3, G4, and G6). of PAMAM dendrimer. Also we utilized the same model to investigate the linker formation in overcharged DNA-G2 PAMAM dendrimer complexes. Finally, we applied our approach to investigate the morphologies formed when a ssDNA and dsDNA wrapped around many spheres of G2 and G4 PAMAM dendrimer.

Chapter 2: METHODS

We used Brownian dynamics simulations of a dissipative bead model of DNA and dendrimers to study the structure and dynamics of multiple DNA-dendrimer complexes. We also utilized various analysis methods to characterize these complexes. In what follows we describe system compositions, simulation and analysis methods details.

2.1. Brownian Dynamics Simulations

Brownian motion is the random motion of particles suspended in a fluid resulting from their collisions with the fast-moving atoms or molecules of the host-medium. It was named after Robert Brown who observed a pollen grain suspended in water and moved on its own. On a different occasion, Brown observed similar motion with dust particles. The latter observation ruled the hypothesis that pollen grain motion was due to the pollen grain being alive. However, he was unable to explain the underlying physics principles of such motion. Albert Einstein discovered later on that the random thermal motions of fluid molecules striking the microscopic particle and causing it to undergo a random diffusion [95, 96].

BD is a dynamic simulation method that can be used to model the time-evolution behavior of a given molecular system[97, 98]. Because of the large number of individual atoms in a biomolecular system of interest, it is often not feasible to study these systems using all-atom MD simulations. Therefore, in BD simulation the solvent (water) is modeled using continuum models, along with a simplified description of the macromolecules. In particular, the thermal motion and hydrodynamic drag of the solvent are replaced by a suitable stochastic force on the macromolecules. Also, the electrostatic interactions of macromolecules with

14

water and ions are replaced by a mean-field approximation in which ion concentrations and dielectric properties of the water one considered. Furthermore, the Brownian model assumes that the solvent damping is very large compared to inertial effects.

We used the scalable Brownian dynamics package, BD_BOX, to perform our multiscale simulations of our primitive models of systems containing significant numbers of DNA and dendrimer molecules. Although BD_BOX provides different modeling approaches such as shape-based coarse graining technique, each dendrimer and nucleotide (or base pair) in a DNA were represented by a single spherical bead[100] [102103]. Each bead in the simulation is characterized by a set of parameters including the hard core radius (R), used to evaluate inter- and intra-molecular excluded volume interactions and long-range attractive interactions between species, the corresponding potential well-depth (ϵ^{LJ}), the central charge (Q), and optionally the mass (m). The potential energy of a system of spherical subunits is described by a force-field that includes a sum of bonded and non-bonded interactions.

2.1.1. Bonded Interactions

All particles in the BD_BOX are joined by a connector bond. Each particle (except the terminal ones) is joined to its two neighbors to form linear chain. Any particle may be joined to an arbitrary number of other particles. The sum extends over all the pairs of connected particles. Connectors behave mechanically as springs with an associated potential V_{ij}^{bond} that depends on the distance between the two joined particles, equal to the length of the spring, $|\vec{r}_{ij}| = |\vec{r}_i - \vec{r}_j|$, where

$\vec{r}_i$ is the position vector of the *i-th* bead. BD_BOX adopts the following spring potential to simulate the DNA molecules.

$$V_{ij}^{bond} = -\frac{1}{2} H r_{max}^2 \ln \left(\frac{r_{max}^2 - r_{ij}^2}{r_{max}^2 - r_0^2} \right) \tag{2.1}$$

$$-\frac{1}{2} H r_{max} r_0 ln \left(\frac{(r_{max} + r_{ij})(r_{max} - r_0)}{(r_{max} - r_{ij})(r_{max} + r_0)} \right)$$

Where H is the force constant, r_0 Is the equilibrium bond length, and r_{max} is the maximal bond length[100, 103]. The equilibrium bond length r_0, the maximum bond length r_{max} and the force constant H are the three parameters of this general spring potential, which we call "hard-FENE" because it includes, as particular cases, several commonly used spring types. When $r_0 \rightarrow \infty$ (in practice, a sufficiently large number), it reduces to $V_{ij}^{bond} = \frac{1}{2} H (r_{ij} - r_0)^2$, proper of a Hookean (Fraenkel)[104] spring that is usually employed with a large value of H to to represent stiff bonds with an equilibrium length r_0. Furthermore, with $r_{max} \rightarrow \infty$ and $r_0 = 0$ we Have $V_{ij}^{bond} = \frac{1}{2} H r_{ij}^2$, which is the potential associated with a Gaussian distribution of the spring length, with $\langle r_{ij}^2 \rangle = 3 k_B T / H$ as used in the Rouse model of linear polymer chains composed of Gaussian subchains[105]. The Rouse model with a linear force and infinite extensibility is inappropriate when external agents, particularly strong flows, stretch the chain and the distribution is not Gaussian. For those cases, the most popular choice is the FENE (finitely extensible, nonlinear elastic; warner)[106] spring, whose potential, $V_{ij}^{bond} = -\frac{1}{2} H r_{max}^2 \ln(1 - r_{ij}^2 / r_{max}^2)$ is a special case of equation 2.1 for $r_0 = 0$. For the spring potential as for other pairwise potentials depending on the distance between elements, the forces acting on the two elements are given by

$$\vec{F}_i = -\vec{F}_j = \left[\frac{dV(r_{ij})}{dr_{ij}}\right]\vec{r}_{ij}/r_{ij} \qquad (2.2)$$

The angles, φ_{ijk}, between two neighbor springs joining beads i and j, and j and k, have the potential shown in equation (2.3). Where k_φ is a bending force constant and φ^0 is the equilibrium value of the angle[107].

$$V_{ijk}^{angle} = \frac{1}{2}k_{\varphi ijk}(\varphi_{ijk} - \varphi_{ijk}^0)^2 \qquad (2.3)$$

If ij, jk, and kl are three consecutive bonds, internal rotation around the jk bond can be represented by a potential V_{ijkl}^{dihe} exhibited in equation (2.4) or formula (2.5). θ_{ijkl} is called the dihedral angle, k_θ is the force constant and θ_0 is the equilibrium angle[100, 107]

$$V_{ijkl}^{dihe} = \frac{1}{2}k_{\theta ijkl}(\theta_{ijkl} - \theta_{ijkl}^0)^2 \qquad (2.4)$$

$$V_{ijkl}^{dihe} = \frac{1}{2}k_{\theta ijkl}\left(1 + \cos(\delta_{ijkl})\cos(m_{ijkl}\theta_{ijkl})\right) \qquad (2.5)$$

Where $\delta_{ijkl} = 0$ or $\delta_{ijkl} = \pi$ and $m = 1,2,\dots,6$.

Figure 2.1 below shows a representation of the bead-spring model used in this study and illustrates the plane and dihedral angles.
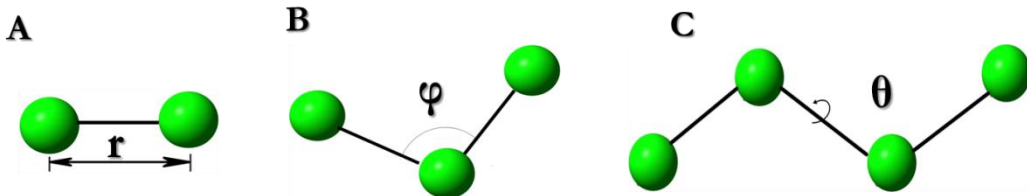
Figure 2.1: Representation of the DNA bead-spring model. A panel shows the bond length joins the beads with equilibrium length of r_0. B panel illustrate the plane angle between two bonds. C panel exhibits the dihedral angle between three bonds.

2.1.2. Non-Bonded Interactions

Non-bonded interactions in BD_BOX include two other kinds of pairwise intramolecular potentials. The first non-bonded potential is given by equation (2.6) and known as the Debye-Hückel mean field approximation of electrostatic potential (shown in Figure 2.2). This approximation is used to model the screened electrostatic interactions between charged elements in electrolyte media. In short, two spherical subunits with radii R_i and R_j and central charges Q_i and Q_j interact via pairwise additive potentials of the form[100]:

$$V_{ij}^{el} = \frac{Q_i Q_j}{4\pi\epsilon_0\epsilon(1 + \kappa R_i)(1 + \kappa R_j)r_{ij}} e^{-\kappa(r_{ij}-R_i-R_j)} \tag{2.6}$$
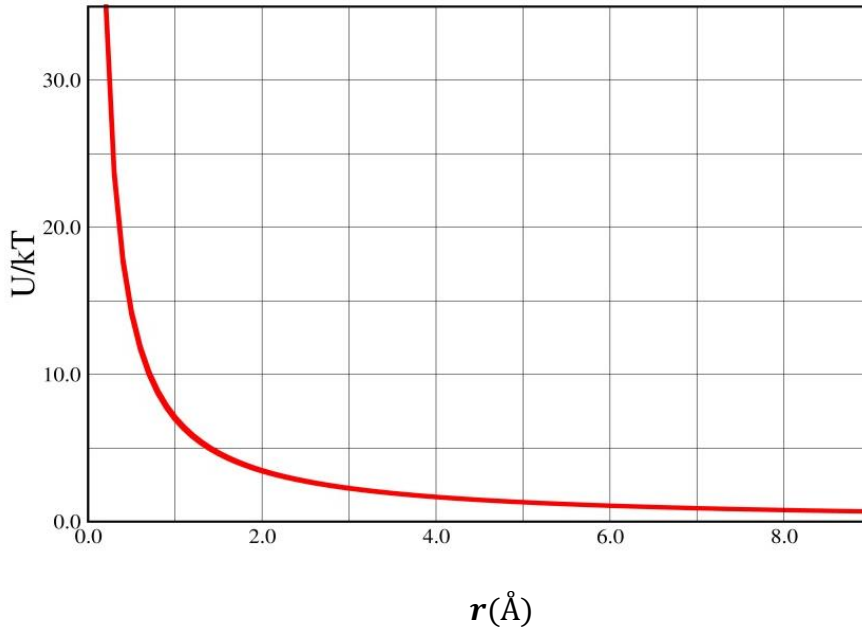
Figure 2.2: The Debye-Hückel potential. A potential used to model screened electrostatic interactions between two charged spheres.

where ϵ_0 is the vacuum permittivity (8.854×10^{-12} C^2/Nm^2) , ϵ is the dielectric constant of water, r_{ij} is the separation distance between charges, κ is the inverse of the Debye screening length which measures the shielding effect that the solution ions exert on the electrostatic interactions between beads. It is defined by:

$$\kappa^{-1} = (8\pi c_s l_B)^{-\frac{1}{2}} \tag{2.7}$$

The Bjerrum length l_B measures how far away two charges have to be so that the attractive or repulsive electrostatic energy is balanced by the randomizing effects of thermal energy. Therefore, it characterizes the strength of the screened electrostatic interaction. It is given by:

$$l_B = \frac{e^2}{\varepsilon k_B T} \tag{2.8}$$

Where $k_B T$ is the thermal energy and c_s is the bulk salt concentration[1, 108, 109]. For water at room temperature $l_B = 7.14$ Å.

The second non-bonded pairwise potential is Lennard-Jones potential (Figure 2.3). It is used for excluded-volume interactions. The repulsive interactions between subunits at small separations and attractive interactions at large separations are evaluated using standard Lennard-Jones formula:

$$V_{ij}^{LJ} = 4\epsilon_{ij}^{LJ} \left[\left(\frac{\sigma_{ij}^{LJ}}{r_{ij}} \right)^{12} - \left(\frac{\sigma_{ij}^{LJ}}{r_{ij}} \right)^{6} \right] \tag{2.9}$$

Where $\epsilon_{ij}^{LJ} = \sqrt{\epsilon_i^{LJ}\epsilon_j^{LJ}}$ is the well depth and $\sigma_{ij}^{LJ}=R_i + R_j$. It is also possible to model only purely repulsive interactions, without the long-range term.

19
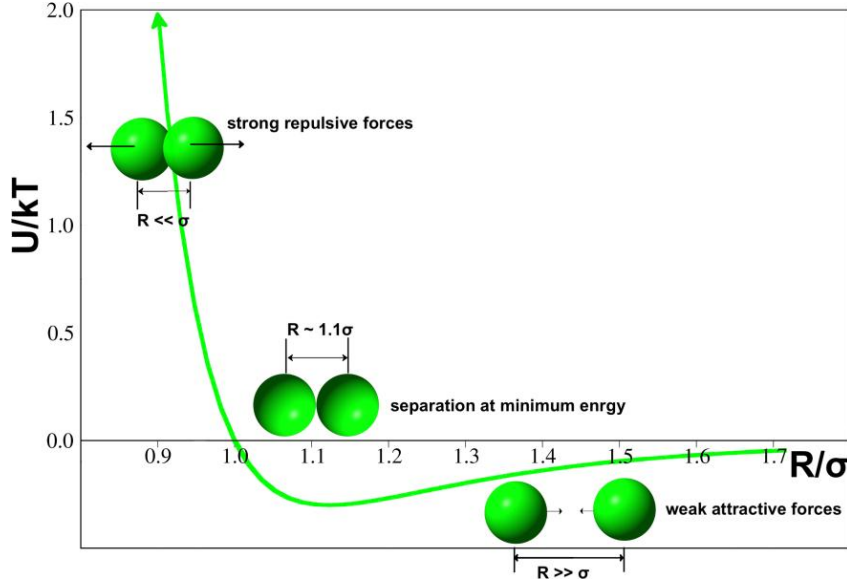
Figure 2.3: Lennard-Jones potential. The beads experience strong repulsive forces when they are overlapped and weak attractive force when they are separated.

BD trajectories of bead models in a viscous solvent can be created with the Ermark-McCammon[110] algorithm or the two step predictor-corrector algorithm [111]. According to Ermarck-McCammon algorithm the position of the *i-th* bead after time Δt is given by:

$$\vec{r}_i = \vec{r}_i^0 + \frac{\Delta t}{k_B T} \sum_{j=1}^{j=N} D_{ij}^0 \vec{F}_j^0 + \vec{R}_i \qquad (2.10)$$

Where $\vec{r}_i^0$ is a three dimensional vector to describe the initial position of the *i*-th bead, k_B is the Boltzman constant, T is the temperature, *N* is the number of spherical beads in the system, D_{ij}^0 is the 3×3 element of the 3N × 3N diffusion tensor computed for the initial configuration of particles, $\vec{F}_j^0$ is the total force acting on the *-i*th bead and $\vec{R}_i$ is a Gaussian random vector with a zero mean, the presence of this vector leads to nonphysical overlaps between beads when the separation between any two beads is smaller than the sum of their hard-core radii even when the Lennard-Jones interactions are evaluated. Therefore, time step in

20

BD simulations should be sufficiently short, so that the forces acting on the diffusing beads do not change significantly in one simulation time step.

2.2. Model and Simulation Details

In this study, a dendrimer is modeled by a positively charged sphere, while a DNA chain is represented by a bead-spring model in which nucleotides of single-stranded DNA (ssDNA) chain (or nucleotide pairs for double stranded DNA (dsDNA)) are modeled by beads that are connected together by an elastic spring, with spring constant of 0.6 kcal/mol.Å^2, with persistence length of 164Å. Figure (2.4) shows the mapping of G4 dendrimer and dsDNA.
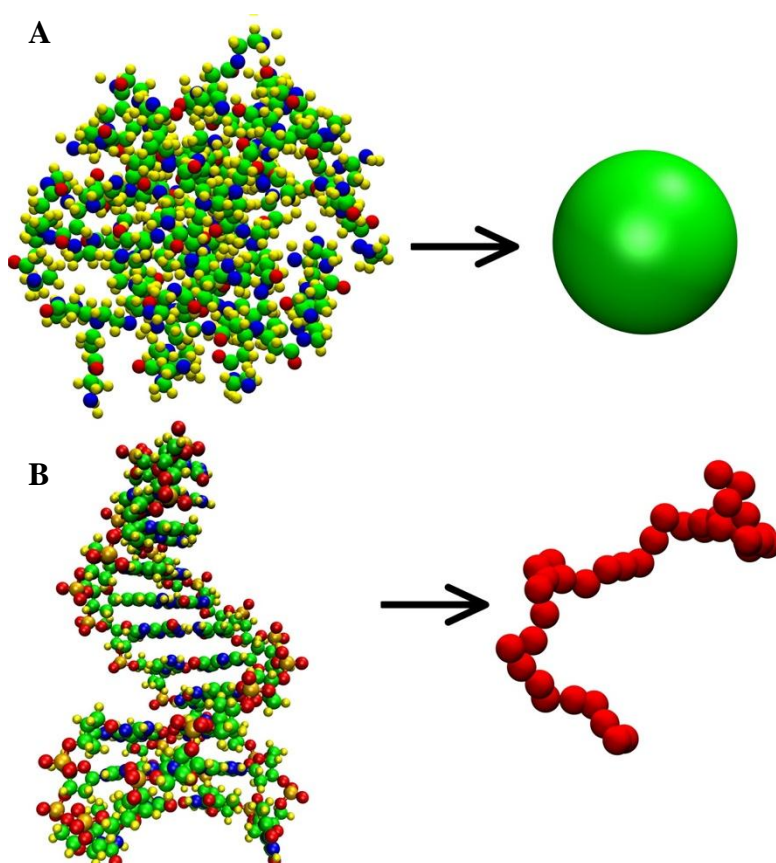
Figure 2.4: The bead spring model used in this study. A: all atom structure of G4 PAMAM dednrimer mapping into one sphere of radius 22.5 Å. B: all atom structure of dsDNA is mapped into a chain of bonded beads each of radius 2 Å. The colors indicate the types of atoms in the all-atom structure; blue, green, yellow, orange and red for nitrogen, carbon, hydrogen and phosphorous, respectively.

21

The model of DNA is based on a linear flexible polyelectrolyte model previously used to study the complexation between a linear flexible polyelectrolyte and macroions[112, 113]. This model describes dsDNA as a freely jointed chain of charged hard spheres each of them has a radius of 2.0Å and a charge of –2e connected by harmonic bonds of spring constant of 0.576 kcal/(mol.Å^2). All the BD simulations were carried out using BD-BOX program[100] which utilized Ermak-McCammon algorithm with 20fs time step to find the Brownian trajectories of the particles solvated in water with viscosity 0.01 Poise and dielectric constant of 78.54. Some of the relevant physical properties of the PAMAM dendrimer investigated are shown in the following table:

Table 1: a summary of the physical properties of G2, G4, G6 and G8 PAMAM dendrimers. here r_0 is the radius of gyration of the dendrimer; n_{exp} is the experimentally determined number of dendrimers bound per DNA molecule; Z is the number of surface charge groups on each dendrimer; the charge ratio (rcharge) is defined as the ratio between the charge groups on the dendrimer and the phosphate groups on the DNA, i.e. for each dendrimer , rcharge $= n(NH_3^+)/n(PO_4^-)$; z_{chain} is the number of charges on each DNA chain (=8662 for 4331bp dsDNA) and l_{iso} is the length of the double stranded DNA (dsDNA) required to neutralize the charge of each dendrimer generation.

Dendrimer	R_0(Å)	n_{exp}	Z(e)	$n_{exp}Z_D/Z_{chain}$	l_{iso}(Å)
G2	14.5	318	16	0.58	27.2
G4	22.5	140	64	1.03	108.8
G6	33.5	16	256	0.47	435.2
G8	48.5	5	1024	0.59	1740.8

2.3. The Effect of Salt Concentration

The salt concentration is taken into consideration through the inverse of Debye screening length $\kappa^{-1} = (8\pi c_s l_B)^{-\frac{1}{2}}$, where $l_B = \frac{e^2}{\varepsilon k_B T}$ is the Bjerrum length, $k_B T$ is the thermal energy and c_s is the salt concentration[1]. Increasing the salt concentration has the same effects as increasing pH or increasing the valence of the salt ions which weakens the attractions between the negative charges on the DNA and the positive charges on the dendrimer. We carried out various BD simulations for generations 2 and 3, 4 and 6 at different salt concentrations (10-1000mM), Tables 2 and 3 below shows the composition of each system for dsDNA and ssDNA, respectively:

Table 2: The composition of dsDNA-dendrimer complexes used in the BD simulations.

G	No of DNA beads	No of dendrimer spheres	Radius of dendrimer bead(Å)	Dendrimer charge(e)	r_{charge}	Length of simulation (µs)
2	19	1	14.5	16	0.42	2.5
3	38	1	15.8	32	0.42	2.5
4	38	1	22.5	64	0.84	2.5
6	38	1	33.5	256	3.4	2.5

Table 3: The composition of ssDNA-dendrimer complexes used in the BD simulations

G	No of DNA beads	No of dendrimer spheres	Radius of dendrimer bead(Å)	Dendrimer charge(e)	r_{charge}	Length of simulation (µs)
2	19	1	14.5	16	0.84	2.5
3	38	1	15.8	32	0.84	2.5
4	38	1	22.5	64	1.7	2.5
6	38	1	33.5	256	6.7	2.5

The number of dendrimer and DNA beads are taken to get the same r_{charge} of that considered by Shi Yu and Larson[95]. The charge ratio r_{charge} is defined by equation (2.11):

$$r_{charge} = \frac{number\ of\ positive\ charges\ on\ denrimer}{number\ of\ negative\ charges\ on\ DNA} \quad (2.11)$$

2.4. Order parameter (η)

To quantitatively study the structure of DNA during the simulation we define the order parameter η, [95, 114, 115]:

$$\eta = \frac{|\sum_i \vec{r}_{i-1,i} \times \vec{r}_{i,i+1}|}{N} \quad (2.12)$$

Where $\vec{r}_{i,i+1} = \frac{\vec{r}_{i,i+1}}{|\vec{r}_{i,i+1}|}$, $\vec{r}_{i,i+1} = \vec{r}_{i+1} - \vec{r}_i$, N is the number of DNA beads, $\vec{r}_i$ is the ith DNA bead position. Equation (2.12) only accounts for the cross product of adjacent vectors $\vec{r}_{i-1,i}$ and $\vec{r}_{i,i+1}$ for which the $(i-1)^{th}$, i^{th} ,$(i+1)^{th}$ beads are all DNA bead neighbors that are adsorbed on the dendrimer.

2.5. Toroidal Parameter τ

The morphologies of higher order complexes resulted from the DNA and dendrimers have different forms according to the dendrimer generation. To distinguish the rod-like and toroidal DNA-dendrimer structure, we evaluated the *toroidal parameter τ* defined as [116]

$$\tau = \langle \frac{1}{N_c - 2} \left[\sum_{\alpha=x,y,z} \left(\sum_{i=2}^{N_c-1} \frac{(\vec{r}_{i-1,i} \times \vec{r}_{i,i+1})_\alpha}{|\vec{r}_{i-1,i} \times \vec{r}_{i,i+1}|} \right)^2 \right]^{1/2} \rangle \quad (2.13)$$

Where $\vec{r}_{i-1,i}$, $\vec{r}_{i,i+1}$ are the vectors of two successive bonds and N_c is the number of complexes. The toroidal parameter approaches 1 when the beads are arranged along an ideal toroid and fluctuate around $\frac{1}{N_c-2}$ for a random

24

distribution[117]. We carried out several BD simulations to study how the dendrimer

generation and the length and stiffness of DNA chain affect the structure of DNA-

dendrimer complex formed. Table 4 shows the properties of the systems used:

TABLE 4: The composition of the system used to study the aggregates of DNA-dendrimers.

System number	DNA type	G	Number of dendrimer beads	Number of DNA beads	Length of simulation (μs)	Spring constant (kcal/mol.$\mathring{A}^2$)
1	dsDNA	2	100	1362	8.0	0.6
2	ssDNA	2	100	1362	8.0	0.6
3	dsDNA	4	43	1330	5.0	0.6
4	ssDNA	4	43	1330	5.0	0.6
5	dsDNA	2	10	136	6.0	0.6
6	dsDNA	2	10	136	6.0	0.06
7	dsDNA	2	10	136	6.0	2.6
8	dsDNA	2	50	681	4.0	0.6
9	dsDNA	2	100	1362	4.0	0.6

Chapter 3: RESULTS AND DISCUSSION

The results obtained are classified according to the number of dendrimer spheres participating in the simulation. Section 3.1 discusses the complexes between dendrimers of various generations (G2, G3, G4 and G6) and ssDNA or dsDNA at different salt concentrations. Section 3.2 examines the structures of aggregates formed between a single and double stranded of DNA and multiple spheres of dendrimer.

3.1 The Complexation between DNA and a Single Dendrimer.

3.1.1. Salt Concentration Effects

Ideality is a concept used for solutions only if the interactions between the particles are negligible. If the amount of the solute in the solution is significant the solution is considered to be non-ideal with ideality increasing with increasing the solute concentration[118]. The electrostatic interactions are the main forces act on the DNA-dendrimer complexation so this complexation will be affected by the physiologic salt concentration. As described in chapter 2, we used a bead-spring model of DNA and represented dendrimer as a single bead to study the effect of salt concentration on the complexation between DNA chain and dendrimer bead.

Table 5: The Debye screening length (κ^{-1}) evaluated at different salt concentration levels (c_s).

$c_s \ (mM)$	10	50	100	200	300	400	500	600	700	800	900	1000
κ^{-1}(Å)	0.03	0.08	0.11	0.15	0.18	0.2	0.23	0.25	0.27	0.29	0.3	0.33

The salt concentration is taken into consideration through the inverse of Debye screening length (κ^{-1}) at temperature of 298 K and salt concentration (c_s) as in Table 5.

To study the effect of salt concentration on the structure and dynamics of the DNA-dendrimer complex, we carried out various BD simulations for double and single stranded DNA of spring constant of 0.6 kcal/mol.$\mathring{A}^2$ and persistence length of 164$\mathring{A}$, with generations 2, 3, 4, and 6 dendrimers at different salt concentrations (10 - 1000mM). In subsequent subsections we discus and analyze these simulations.

3.1.2. Double Stranded DNA

We carried out BD simulations for four systems of dsDNA with G2, G3, G4 and G6 PAMAM dendrimers. In G2-19 bp DNA system, G2 has 16 protonated amines while dsDNA is represented by 19 beads to give 38 negative charges. In G3-38 bp DNA system, G3 has 32 positive charges and dsDNA has 38 negative beads with total negative charge of 76e. Also 38 negative beads of charge of -76e substitute the dsDNA beads in G4-38bp dsDNA and a sphere of 64e charge represent G4 dendrimer. The last system of G6-38bpDNA, the charge of dendrimer was 256e and the charge of dsDNA is -76e. All the characteristics of the spheres and beads of PAMAM dendrimers and dsDNA are shown in Table 2 above.

We see in Figure 3.1snapshots from the simulations of the described systems at 10mM. We can see that the dsDNA wraps around PAMMA dendrimers in different manners. We evaluated r_{charge} as in equation (2.11). The charge ratio r_{charge} is less than unity for the G2-19 bp DNA complex, G3-38 bp DNA and G4-38 bp DNA, while r_{charge} is more than unity for the G6-38 bp DNA

complex. At 10 mM, in complexes formed by the dsDNA and G2, G3 and G4 where the r_{charge} is less than unity the dsDNA does not wrap completely on the dendrimer because the positive charge of the dendrimer (G2, G3 and G4) is less than the negative charge of dsDNA leaving excess dsDNA beads free without participating in the dsDNA-dendrimer complex. However in the complexes where
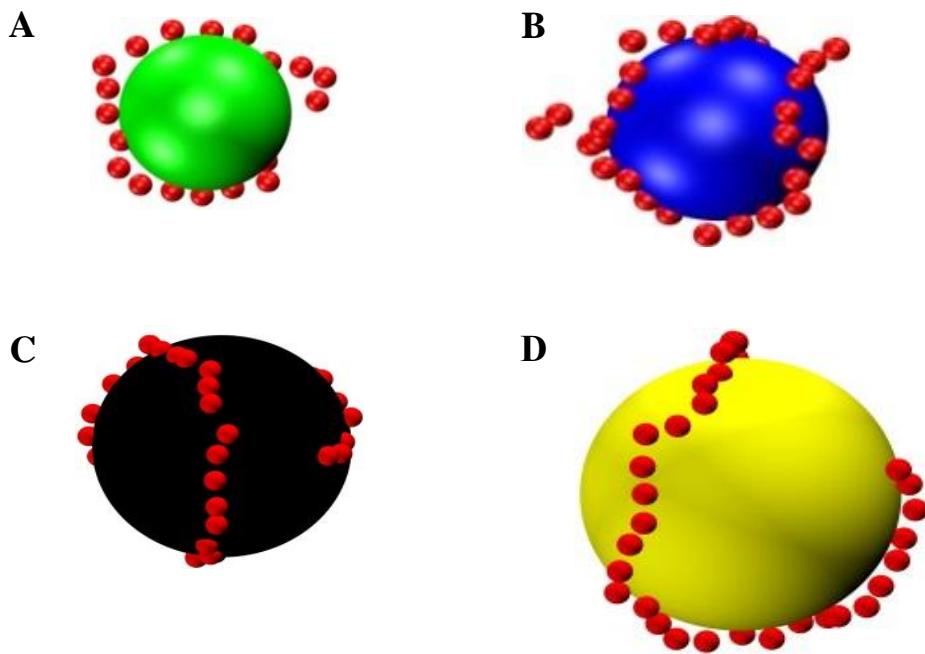
Figure 3.1: Snapshot of dsDNA condensed by G2(green) and G3(blue), G4(black) and G6(yellow) dendrimer at low salt concentrations.

r_{charge} is more than unity (e.g. the complex formed by G6 and dsDNA), the negative charge of dsDNA (76 e) is less than the positive charge of G6 (256 e) so all the dsDNA beads are absorbed onto the G6 dendrimer leaving no free bead. These observations are in agreement with findings of Nandi and Maiti in their all-atom MD simulations[119]. It is worth mentioning here that G6 is of similar in size and charge to a histone octamer and the complex resulting from G6 and dsDNA seems to be similar to those in nucleosome despite that DNA lengths are only half of that in a nucleosome[120].

In systems of G2-, G3-, G4- and G6-dsDNA, we calculated the distances between center of mass of dsDNA and the center of mass of each dendrimer sphere participating in the simulations (G2, G3, G4 and G6) and plotted them as a function of salt concentration as shown in Figure 3.2. At low salt concentrations (10, 50, 100, 150 mM) the dsDNA is at the closest distance with G2, G3, G4 and G6 which indicates that the dsDNA wraps well around PAMAM dendrimer to form compact complex. Whereas at high salt concentrations (200-1000mM), dsDNA does not form complexes with G2, G4 and G6 so it becomes free far away from the dendrimer due to the high electrostatic screening effects. As we see in Figure 3.2, G3 has different behavior where the dsDNA start to far away from G3 at salt concentration larger than 300 mM, since the charge of G3 increase largely comparing to G2 but its size increases slightly so there are a plenty of charge in a small size which yields strong electrostatic interactions with dsDNA which wraps strongly around G3 dendrimer.
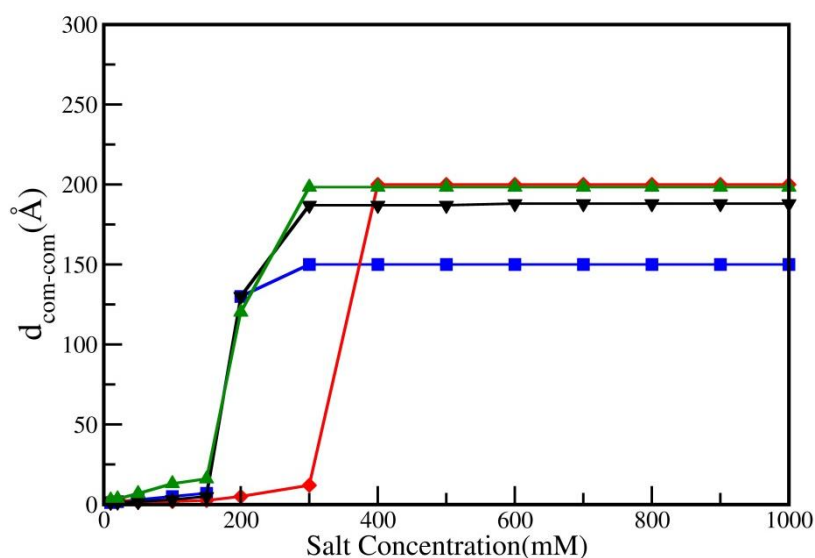
Figure 3.2: the distance between dsDNA-center of mass and dendrimer-center of mass for various salt concentrations. The blue, red, black, and green curves represent G2, G3, G4 and G6 respectively.

To study the number of dsDNA beads adsorbed on each of the dendrimer spheres of generations 2, 3, 4 and 6, we calculated the fraction of absorption ω, which is defined as the ratio between the number of DNA beads that are in the vicinity of dendrimer and the total number of the DNA beads.

The values of ω as a function of salt concentration are shown for different complexes in Figure 3.3. At low salt concentration, ω increases with increasing dendrimer generation. Generations 4 and 6 bind to a larger number of DNA beads than the low dendrimer generations (G2 and G3) since the higher generation dendrimers (G4 and G6) are larger than the low generation dendrimers, they have lower curvature and higher charge which in turn allow the DNA to bend and wrap around them more easily than the low generations. So increasing the dendrimer generation or increasing the size of the dendrimer leads to an increase in the number of DNA beads adsorbed on the dendrimer. This agrees with findings obtained by the theoretical model of Qamhieh et al. [1].
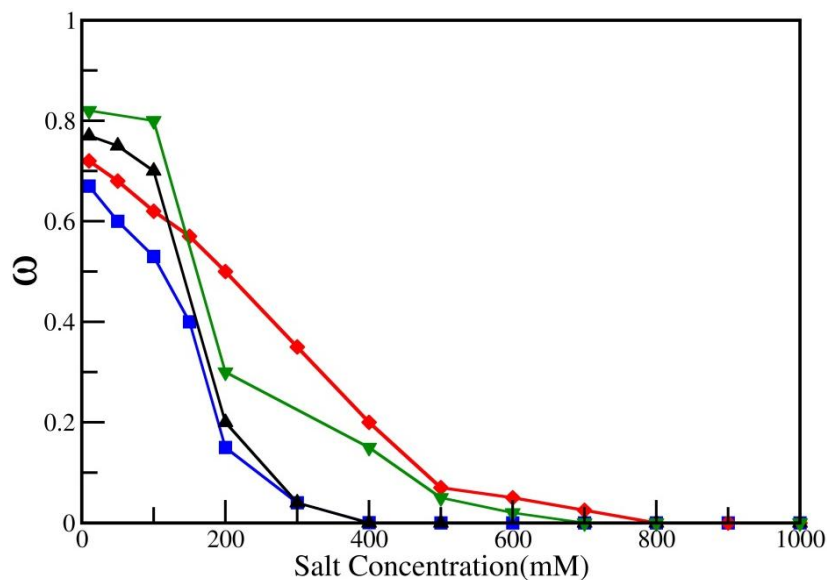
Figure 3.3: Fraction ω of adsorbed dsDNA beads in dendrimer-DNA complexes as a function of salt concentration. Blue, red, black, and green curves represent G2, G3, G4 and G6 respectively.

The values of ω at high salt concentrations are shown in Figure 3.3. For complexes formed between G2, G3, G4 and G6 and dsDNA, we note that ω decreases with increasing the salt concentration and goes to zero at very high salt concentration ($c_s \geq 400$ mM for G2 and G4) and it vanishes at c_s larger than 600 mM and 800mM for G6 and G3 respectively. The zero values of ω means that there is no dsDNA beads are adsorbed on the dendrimer sphere. That because the stronger ion screening effects at high salt concentration limit the wrapping of DNA chain around dendrimer. This means that DNA wraps weakly around dendrimer at high salt concentration due to the strong ion screening effects which weakens the electrostatic interactions between DNA and dendrimer, which agrees with the results obtained by Larson. *et*, *al*[95]. We deduce also from Figure 3.3 that G3 behave differently than the other generations (G2, G4 or G6), we see that ω of the dsDNA absorbed on G3 dendrimer still high at large values of salt concentrations(200, 300, 400, 500, 600, and 700mM) before becoming zero at 800, 900 and 1000 mM. comparing to G2, G3 has a large positive charge comparing to its size so the electrostatic attractions between G3 dendrimer and dsDNA is very strong which is not affected easily by increasing the salt concentrations.

Increasing the dendrimer generation does not only increase the degree of DNA adsorption, but also it may affect the shape of DNA wrapping around it. To quantify this observation, we calculated the order parameter (η) which was defined by equation (2.12). The order parameter (η) measures the ordered degree of the wrapping, it is zero when the DNA is straight or when it is randomly coiled, small for disordered complexes, and it will be unity if the DNA were to bend an angle of 90 always in the same direction forming a tight helix[95].
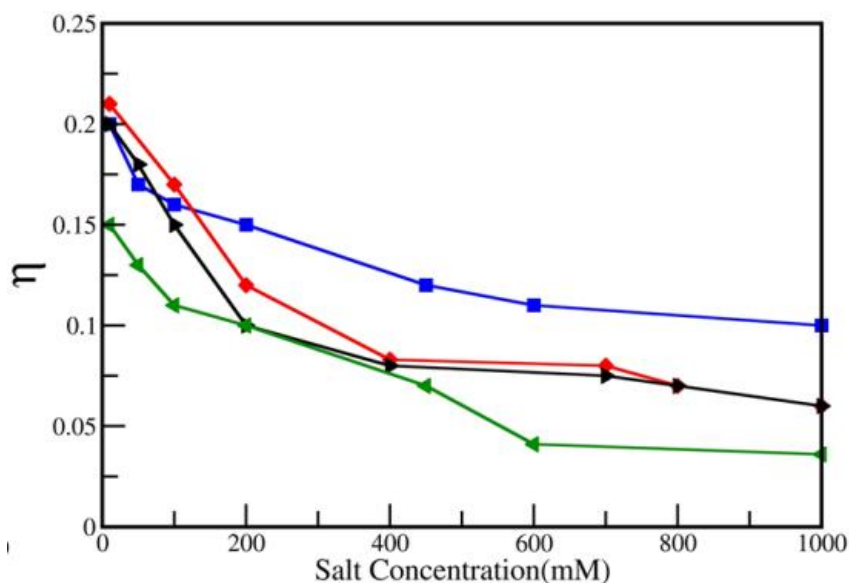
Figure 3.4: The order parameter η in dsDNA-dendrimer complexes as a function of salt concentration. Blue, red, black, and green curves represent G2, G3, G4 and G6 respectively.

As shown in Figure 3.4, the disordered complex is formed when η is around 0.15 for G6 since dsDNA wrap around it in a non-order pattern while for G2 η=0.2 is slightly larger than G6. Hence, the ordering degree of dsDNA wrapping around G2 is larger than that of G6. At high salt concentration, η values become very small which means the dsDNA chain becomes much straighter due to very weak electrostatic attractions between dsDNA and G2, G3, G4 and G6 dendrimers which reduce the bending and wrapping of dsDNA around dendrimer spheres.

3.1.3. Single Stranded DNA

We carried BD simulations of G2, G3, G4 and G6 dendrimers with ssDNA. ssDNA chain is represented by the bead spring model, such that each nucleotide is represented with a bead of radius 2 Å and charge of –e. We ran four systems, G2-19 beads of ssDNA, G3-38 ssDNA beads, G4-38 ssDNA beads and G6-38ssDNA beads. The ssDNA chain that has 19 beads has a total negative charge of 19e,

whereas the total negative charge of the 38beads of ssDNAchain is 38e . As shown in the Table 3, r_{charge} is less than unity for complexes of ssDNA with G2 and G3. while it is larger than unity for G4-ssDNA and G6-ssDNA complexes.
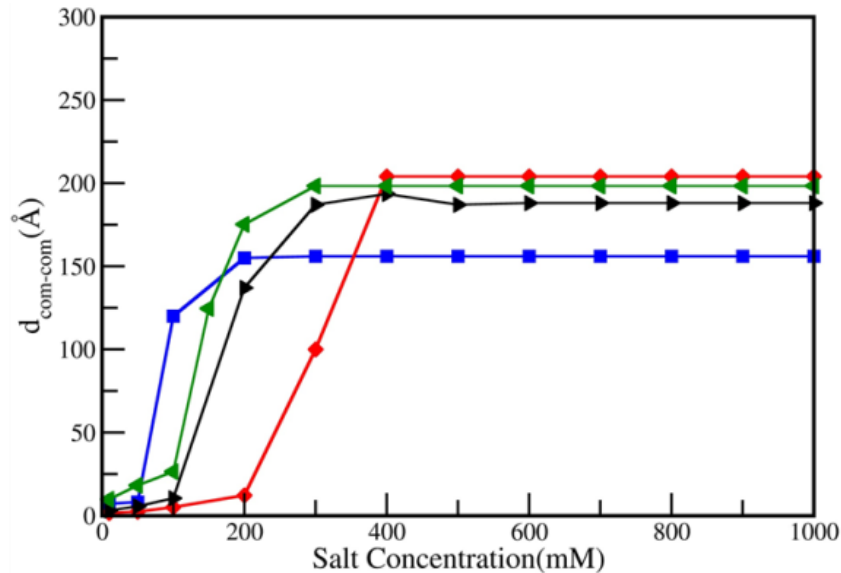
Figure 3.5: Distance between ssDNA-center of mass and dendrimer-center of mass for various salt concentrations. Blue, red, black, and green curves represent G2, G3, G4 and G6 respectively.

The distance between the center-of-mass for the dendrimer to the center-of-mass for the ssDNA chain is plotted versus salt concentration for G2, G3, G4, and G6 dendrimer generationsas shown in Figure 3.5. Like dsDNA, ssDNA becomes free and moves away from the dendrimer sphere of each generation participating in the simulation as salt concentration increases. Figure 3.5 exhibts that the distance between center of mass of ssDNA and center of mass of G3 dendrimer is less that the other generations at high salt concentrations. That because the positive charge of G3 dendrimer(32e) is large relative to its radius (15.8Å) which means that there is a large charge concentrated at the center of small volume which makes the electrostaic interations between G3 dendrimer and ssDNA is very strong comparing with other generations(G2, G4, and G6). Which cannot be screened easily by the ions in the solution.
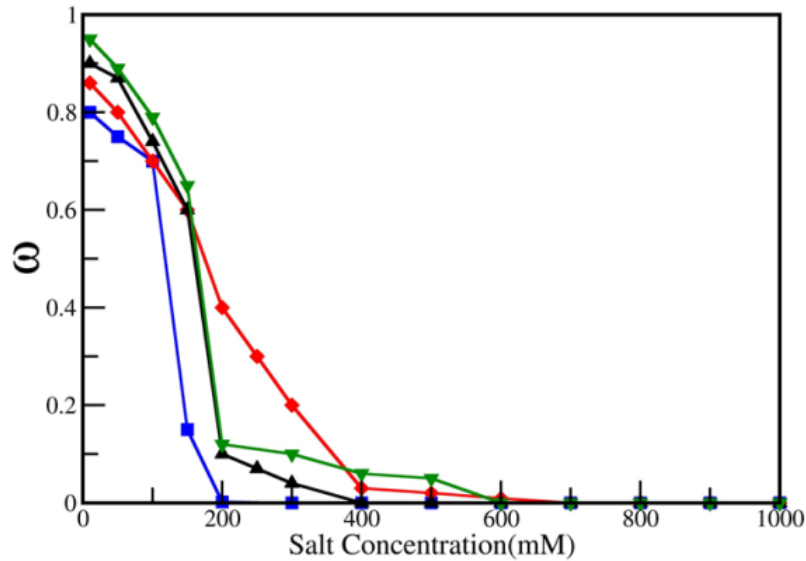
Figure 3.6: Fraction ω of adsorbed ssDNA beads in dendrimer-ssDNA complexes as a function of salt concentration. Blue, red, black, and green curves represent complexing of ssDNA with G2, G3, G4 and G6 respectively.

The fraction of absorbed ssDNA nucleotides for G2, G3, G4 and G6 dendrimer generations is shown in Figure 3.6, at 10 mM the values of ω are increased by increasing the dednrimer generation as in the dsDNA for the same reasons explained previously. By comparing Figures 3.3 and 3.6 with each other, we see that ω of the complex of ssDNA and G2, G3, G4 and G6 generations is larger than that ofG2-, G3-, G4-, and G6-dsDNA. The charge of each bead of the ssDNA is –e which is less than the charge of each of the dsDNA bead (-2e). The number of ssDNA beads participating in the simulation is 19 beads in the G2-ssDNA complexes and 38 beads in the G3-,G4-,G6-ssDNA complexes, the total negative charge of the ssDNA chain (19e or 38e)is less than the total negative charge of the dsDNA(38e or 76e). So the number of ssDNA beads is needed to be adsorbed by a specific dendrimer generartion is larger than the number of dsDNA beads that is required to get the same charge complex of dsDNA and the same dendrimer generation.

34
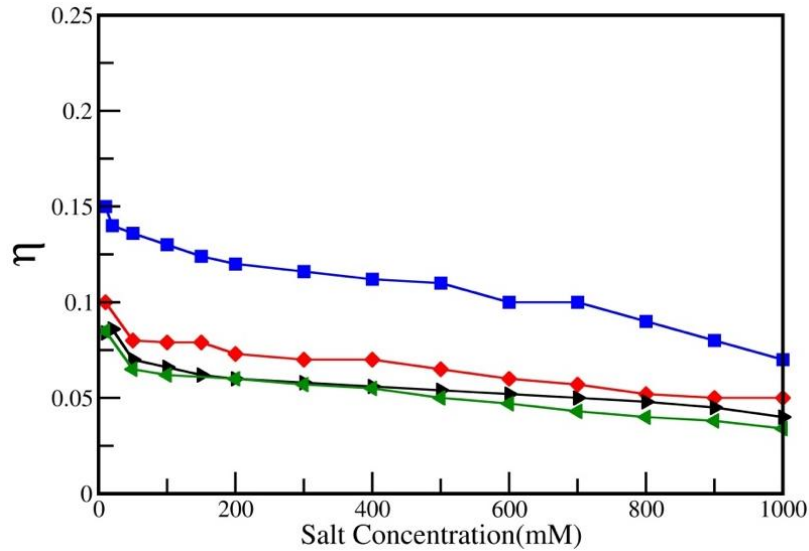
Figure 3.7: Order parameter η in DNA-dendrimer complexes as a function of salt concentration. Blue, red, black, and green curves represent G2, G3, G4 and G6 respectively.

The order parameter η for ssDNA complexes is dcreased by increasing the dendrimer generation which indicates that G4 and G6 dendrimers form disorderd complexes as in the complexes formed byG2, G3, G4, and G6 with dsDNA, but the degree of the disorder in the ssDNA/dendrimer complexes is less than that of the dsDNA/dendrimer complexes, because of its low charge it needs to make more turns around dendrimer.

As the salt concentration is increased the number of ssDNA beads adsorbed on the dendrimer decreases which can be resulted from the values of ω (Figure 3.6), because of the presence of ions which screen the electrostatic interactions between ssDNA and denrimer. The screening effects of ions also prevent the wrapping of ssDNA around the dendrimer so it becomes more strighter at higher salt concentration as can be seen from the values of η in Figure 3.7.

35

3.2. THE COMPLEXATION BETWEEN DNA AND MULTIPLE DENDRIMERS

The structure of the DNA-dendrimer aggregate formed depends on the size of the dendrimer generation, the number of dendrimer spheres and the length of the DNA used in the simulations. According to that, section 3.2 is divided into two sections; section 3.2.1 which examined the linker formation in complexes of three dendrimer spheres and ssDNA or dsDNA. While section 3.2.2 showed the morphologies of the aggregates conform between large number of dendrimers and different chain lengths of single stranded or double stranded DNA.

3.2.1. The Linker Formation in an Overcharged Complex of Three Dendrimers and DNA Chain

We performed several BD simulations of systems each contains three spheres of G2 dendrimer and various number of DNA beads in order to study the absorbtion of DNA by the dendrimer as a function of DNA length. We found that the nonadsorbed beads of DNA (beads that are not participating in the DNA-dendrimer complex) can be spread between tails, loops and linkers. The tail is defined as an unadsorbed part of the DNA chain which has only one adsorbed end. Both ends of loops are adsorbed on the same dendrimer. Ends of linkers are adsorbed on different dendrimers. The snapshots in Figure (3.8) illustrate the morphologies of the resulted aggregates and their dependence on the number of DNA beads(DNA length). These findings are in agreement with those of Lyulin. et al[88], where they have simulated two dednrimers with different values of linear polyelectrlyte (LPE) length.
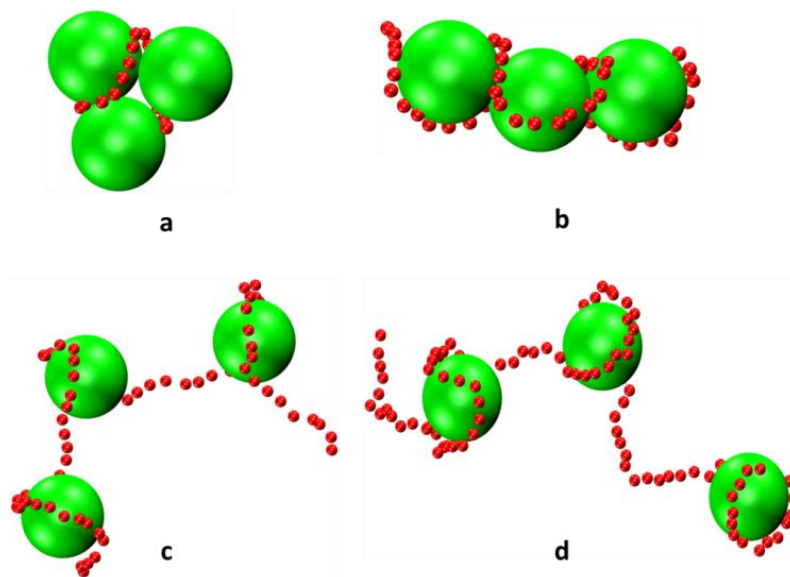
Figure 3.8: Snapshots of aggregates formed of G2 dendrimer with different values of DNA beads. A: 20-DNA-beads, b:45-DNA beads c:70 DNA-beads, d: 100-DNA-beads (3.5 μs BD-simulation)

We studied the motion of DNA chain and G2 dendrimer in the system composed of 3 spheres represent G2 dednrimers and 70 beads represent dsDNA. Figure 3.9 shows the time evolution of the distance between the dsDNA and dendrimer. We note that the distance is stabilized to approximately 20 Å which is comparable to the sum of dednrimer radius and dsDNA radius (14.5+2) Å= 16 Å. This is the closest contact distance between DNA and dendrimer which indicates the DNA wrapp strongly around dendrimer in this case.

In order to understand the dendrimer motion in the complex, we found the distance between each two pairs of dendrimer spheres as shown in Figure 3.10. The first and third spheres are at equal distances all the time while the third sphere is at larger distance apart from them. All of the spheres will be at the minimum distance in the time period (2-2.4 μs).
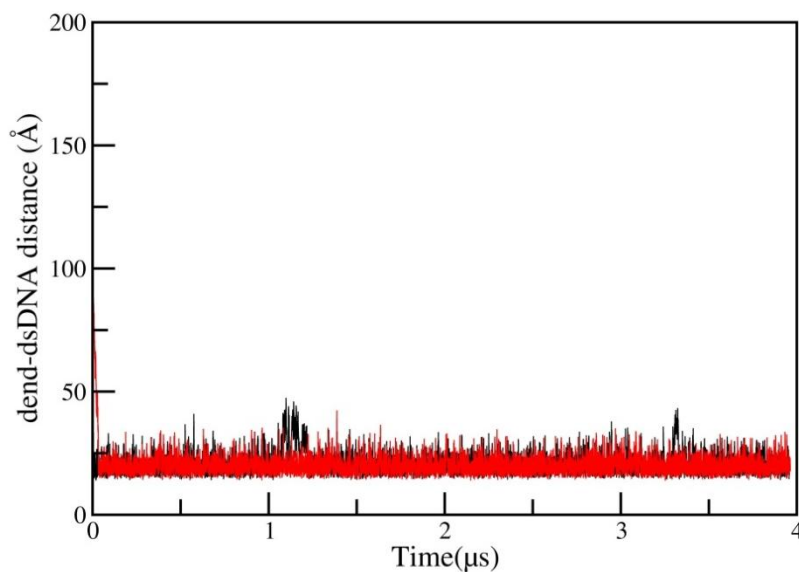
Figure 3.9: The distance between the dendrimer sphere and the dsDNA chain.
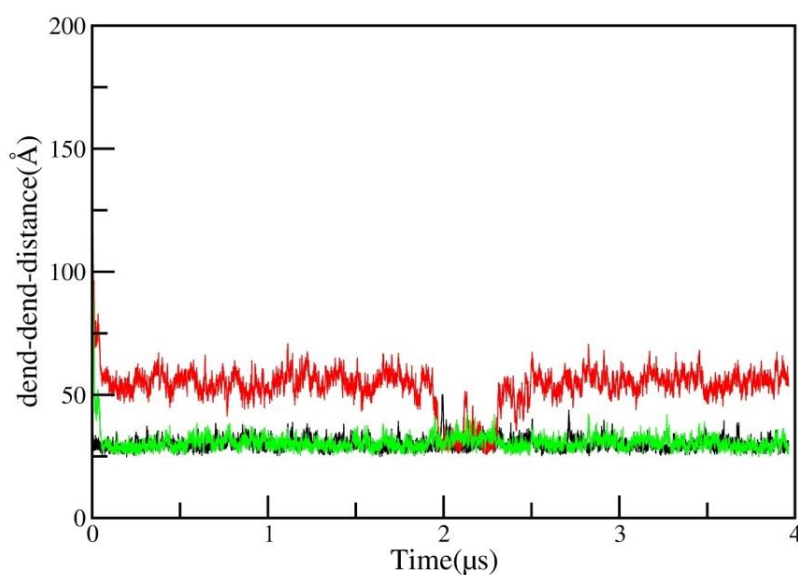
Figure 3.10: The distance between the three dendrimer spheres. Each color represents the distance bween a couple of dendrimers.

Figure 3.11 shows the distance between the ends of the dsDNA chain which is stable around a value of 75 Å. This value is much smaller than the DNA chain length (280 Å) that because parts of DNA chain are bending around dendrimer beads which in turn decreases the end to end distance.
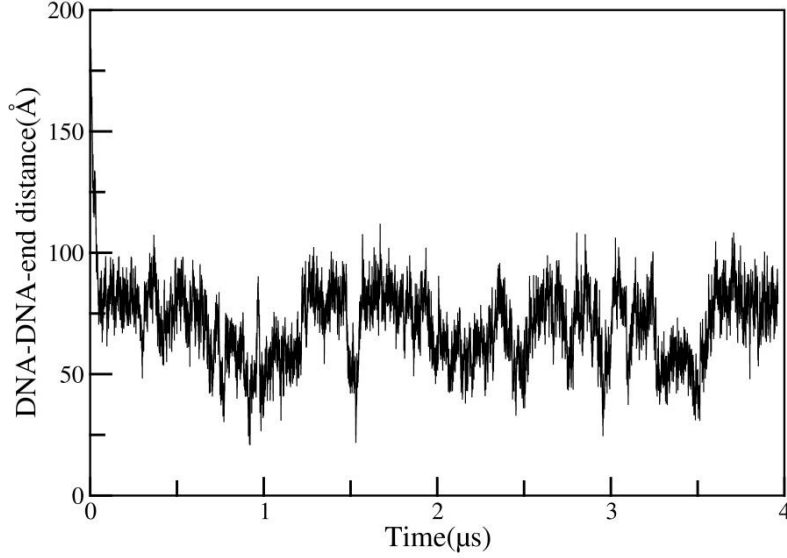
Figure 3.11: The end-end dsDNA distance.

The average number of dsDNA beads that are adsorbed (blue) or not adsorbed on G2 dendrimer sphere (N) is shown in Figure (3.12). The number of dsDNA beads are used in the simulations is termed by N_{ch}. The nonadsorbed dsDNA beads may be as linkers (green line), loops (black line), or tails(red line). For low number of dsDNA beads (*i.e.* N_{ch}=20) all of the beads are adsorbed and there are no linkers, tails or loops. The different types of nonadsorbed parts appear significantly when $N_{ch} \geq 45$ beads and the length of linkers, tails and loops dsDNA is increased by increasing the number of DNA beads participating in the simulations as we see in Figure 3.12. The net charge of the complex ($Q_{complex}$) is calculated according to this formula:

$$Q_{complex} = Q_{G2} + N_{abs}Q_{N_{dsDNA}} \qquad (3.1)$$

Where N_{abs} is the number of DNA beads absorbed on G2 dendrimer or the number of dsDNA beads that are very close to G2 dendrimer, it can be deduced from Figure 3.12. $Q_{N_{dsDNA}}$ is the charge of dsDNA (= -2e) and Q_{G2} is the charge

of G2 dendrimer (=16 e). The number of nonadsorbed part of dsDNA that joined between different dendrimer spheres is called N_{link}, which is calculated and represented by a green line in Figure 3.12. Table 6 shows that when $N_{ch} \geq 20$ beads, the net charge of the complex is negative so that the complex is considered to be overcharged as we see in Table 6.
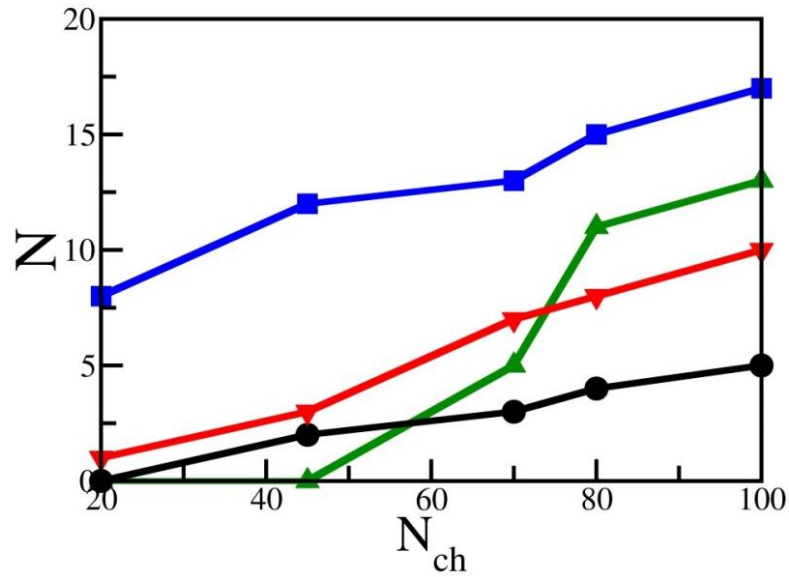
Figure 3.12: The number of dsDNA beads that absorbed (blue line)or not adsorbed by G2 dendrimer sphere as function of dsDNA chain length. The nonadsorbed beads of dsDNA(beads that are not participating in the dsDNA/G2 dendrimer complex can be distributed between tails(red), loops(black) and linkers(green).

Table 6: The charge of G2-dsDNA complex. N_{ch} is the number of dsDNA beads used in simulations, N_{abs} is the number of the dsDNA beads that are adsorbed on each G2 dendrimer and it is get from Figure 3.12. N_{link} is the number of dsDNA beads within one linker that formed between two complexes and it is calculated in Figure 3.12(the green line).

N_{ch}	N_{abs}	Complex Charge	N_{link}
20	8	0	0
45	11	-6	1
70	13	-10	6
80	14	-12	10
100	17	-18	12

The minus sign in the complex charge means that the number of dsDNA beads adsorbed on the G2 dendrimer is larger than that required to neutralize it. This is called overcharging. N_{link} starts appearing when the dendrimer gets close to be overcharged, significantly when N_{ch} is larger than 45.

By comparing Figures 3.12 and 3.13, we deduced that the number of ssDNA beads adsorbed on the dendrimers is less than the number of the adsorbed dsDNA beads for short DNA chain. Whereas, at large number of DNA beads, the adsorption of ssDNA is increased since the charge of each of ssDNA bead is less than the charge of dsDNA bead, so more ssDNA beads one needed to balance the charge of G2 dendrimer.
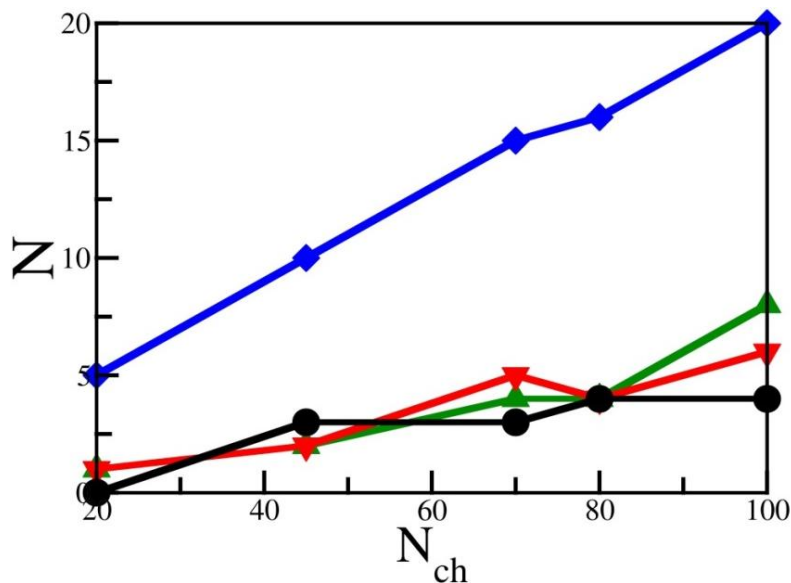
Figure 3.13: The number of ssDNA beads that absorbed (blue line)or not adsorbed by G2 dendrimer sphere as function of ssDNA chain length. The nonadsorbed beads of dsDNA (beads that are not participating in the ssDNA/G2 dendrimer complex can be distributed between tails (red), loops(black) and linkers(green).

Unlike the dsDNA, ssDNA starts to form linkers between G2 dendrimer spheres when the DNA is short (N_{ch}=20 beads). That is because the adsorbed beads of ssDNA are less than that of the dsDNA. The small charge of ssDNA

weakens the electrostatic attraction between it and positive dendrimer so the absorption is less than the dsDNA and the linker formed is larger. Whereas for high N_{ch} (longer chain)the ssDNA forms linkers, circles and tails less than dsDNA because most of the ssDNA are adsorbed on G2 dendrimer and participating in the complex formation, a few number of ssDNA beads still nonadsorbed and form linkers, tails, and loos as we see in Figure 3.14.
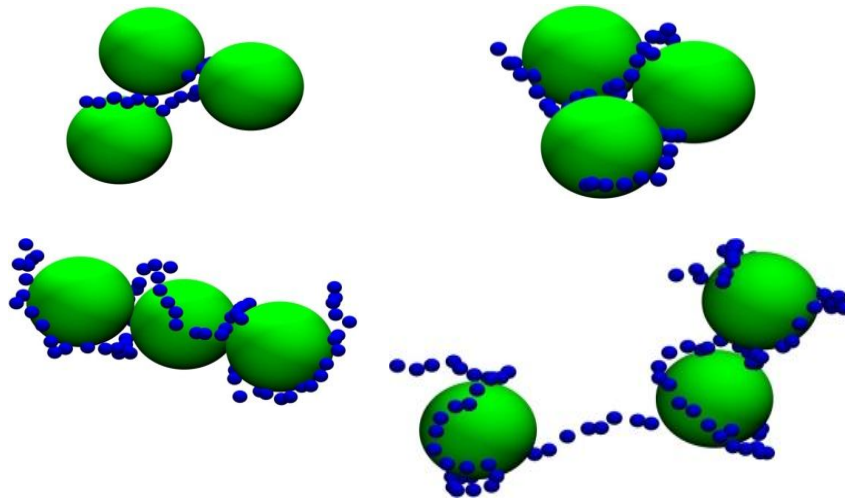
Figure 3.14: Snapshots of complexes formed of 3 spheres of G2 dendrimers with different values of ssDNA beads. a: 20-DNA-beads, b:45-DNA beads c:70 DNA-beads, d: 100-DNA-beads (3.5 µs BD-simulation).

We inferred from the Table 7 that the complex formed of ssDNA and G2 dendrimer is overcharged at $N_{ch} \geq 80$. The complex formed of dsDNA has been overcharged at shorter chain (smaller N_{ch}) than that of ssDNA because the number of dsDNA beads adsorbed on G2 dendrimer is greater than ssDNA beads, which means the negative charge is larger in dsDNA complexes. In short**,** when the total charge of a chain exceeds the total charge of a dendrimer, the structure of DNA-dendrimer will have tails, linkers and circles.

42

Table 7: The charge of G2-ssDNA complex. N_{ch} is the number of ssDNA beads used in simulations, N_{abs} is the number of the ssDNA beads that are adsorbed on each G2 dendrimer and it is get from Figure 3.13. N_{link} is the number of ssDNA beads within one linker that formed between two complexes and it is calculated in Figure 3.13(green line).

N_{ch}	N_{abs}	Complex Charge	N_{link}
20	5	11	1
45	10	6	2
70	15	1	4
80	16	0	5
100	20	-4	7

3.2.2. The Morphologies of the DNA-Dendrimer Aggregates

We studied the complexation of ssDNA and dsDNA with G2 dendrimer by carrying out BD simulations for a system composed of 100 spheres of G2 dendrimers and 1362 nucleotide beads represent ssDNA and dsDNA chains (5448 Å). Also we ran BD simulations of 1330(5320 Å) nucleotides of ssDNA and dsDNA with 43 spheres of G4. We chose these numbers of dendrimer spheres and DNA beads to fit the experimental ratios used by Ainalem et al[96]. Where they utilized cryo-TEM, dynamic light scattering (DLS) and fluorescence spectroscopy to study the morphologies formed between DNA (4331bp) with G1, G2, G4, G6 and G8 PAMAM dendrimers. Our BD simulations show that DNA wrap around dendrimer in different manners according to the dendrimer generation. dsDNA or ssDNA wraps less than one turn around G2 (Figure 3.15) whereas it can wrap more about G4 as shown in Figure 3.17. The smaller curvature of G4 dendrimer and larger charge make it able to interact more effectively with the charged DNA beads. All these findings agree with the experimental results obtained by Ainalem et al[96], and theoretical results of Qamhieh et al[1].

Also the morphologies of the aggregates resulted from the wrapping of DNA around dendrimer depend on the dendrimer generation and DNA type. In our study of the complexation of ssDNA and dsDNA with G2 dendrimer, we observed that the aggregates conformed from the complexation of G2-dsDNA dendrimer trends to be a rod-like structure where the ssDNA does not wrap in the same morphology as illustrated in Figure 3.15.

We calculated the length of the DNA part that are wrapping around the dendrimer sphere (l) by counting the number of DNA beads adsorbed on the dendrimer and multiplying it by the diameter of the DNA bead. We found that for G2-DNA and G4-DNA, l equals to 52Å and 88 Å respectively, which incicates that DNA is wrapping more around G4 dendrimer that G2 dendrimer.

Also we compute the bending energy ($E_{elastic}$) for DNA in G2-and G4-DNA aggregates according to this equation:

$$E_{elastic} \cong \frac{k_B T l_p}{R^2} l \qquad (3.2)$$

Where l is the length of DNA part that are wrapping around dendrimer sphere, $l_p = 164$ Å is the persistence length of the DNA chain, k_B is the Boltzmann constant, T is the temperature and R is the radius of the dendrimer sphere (R=14.5 Å and 22.5 Å for G2 and G4 dendrimers respectively. We found that $E_{elastic}$ equals to 24 and 17.1 kcal/mol for DNA in G2-and G4-DNA aggregates respectively.

The different morphologies arise from G2-ssDNA complexes are accounted for two reasons; one is the low charge of the ssDNA and the other is the high curvature of G2 dendrimer. More ssDNA beads is needed to neutralize

44

the charge of G2 dendrimer compared to the dsDNA but the high curvature of G2 limits the adsorption of ssDNA so the other beads of the ssDNA bend around the dendrimer to form circles. While the low curvature of G4 dendrimer allows the ssDNA beads to wrap more efficient than in G2 as the bending energy is smaller, so the G4-ssDNA form ordered aggregate.
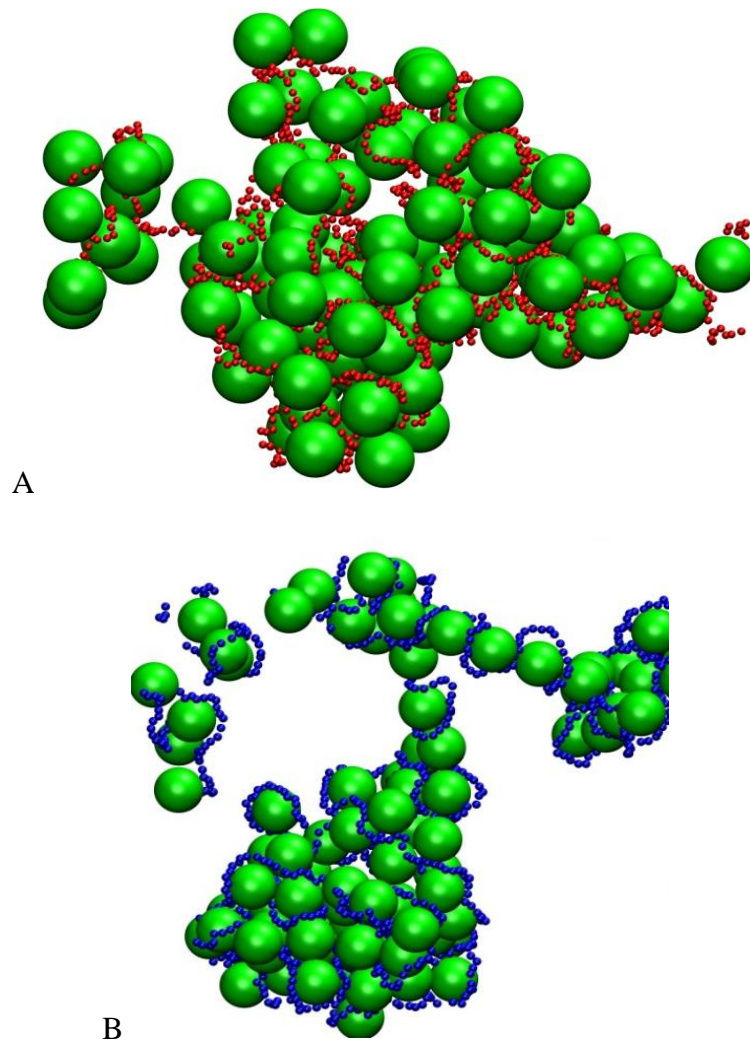
Figure 3.15: Snapshots from the 8.0 μs BD simulation of G2 dendrimer (green beads) and (A) ssDNA (red beads) as well as (B) dsDNA (blue beads).

To analyze the resultant morphology of the aggregate quantitatively, we evaluated the toroidal parameter τ. The high value of τ means that the structure

trends to be a toroid whereas the low τ indicates that the structure is ordered as a rod-like. Figure 3.16 shows the calculated values of τ for ssDNA and dsDNA with G2 as a function of time. For dsDNA τ dropped to around 0.08 which indicates the formation of rod-like structure which has zero toroidal parameter (theoretically), the small deviation from the theoretical value is because the G2-dsDNA complexes are crowded in a small volume which makes some of them to turn around themselves as shown in Figure (3.8. A). τ for G2-ssDNA complexes rose from 0.16 to around 0.2 after 6 μs, which is larger than that of G2-dsDNA complexes but it is not high enough to say that the structure is toroid, this means that ssDNA is not able to wrap around dendrimer in a way to form toroidal structure because as mentioned before, the high curvature of G2 prevents ordered wrapping of the ssDNA around it, the circles formed on one dendrimer can be attracted by other dendrimer so the dendrimers will be crumpled above each other as in Figure 3.15.
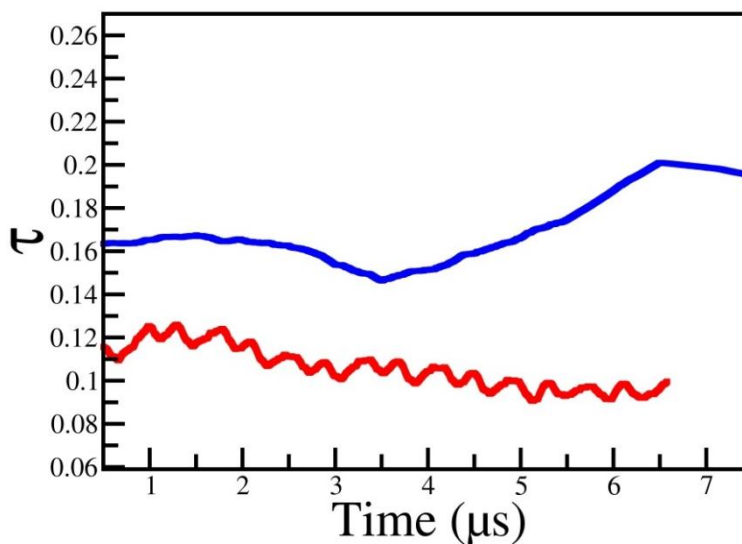
Figure 3.16: The toroidal parameter as a function of time for G2-DNA. Blue line represents ssDNA and red line is for dsDNA.

The low curvature of G4 dendrimer allows the ssDNA wrap more effectively than G2 as explained before, so all the ssDNA beads wrap around G4 in a form like to be a piece of a toroid as Figure 3.17.A shows. The high negative charge of the dsDNA compared to the positive charge of the dendrimer beads participating in the simulation allows not all dsDNA beads combined to the dendrimer which make them free as we see in Figure 3.17. B.
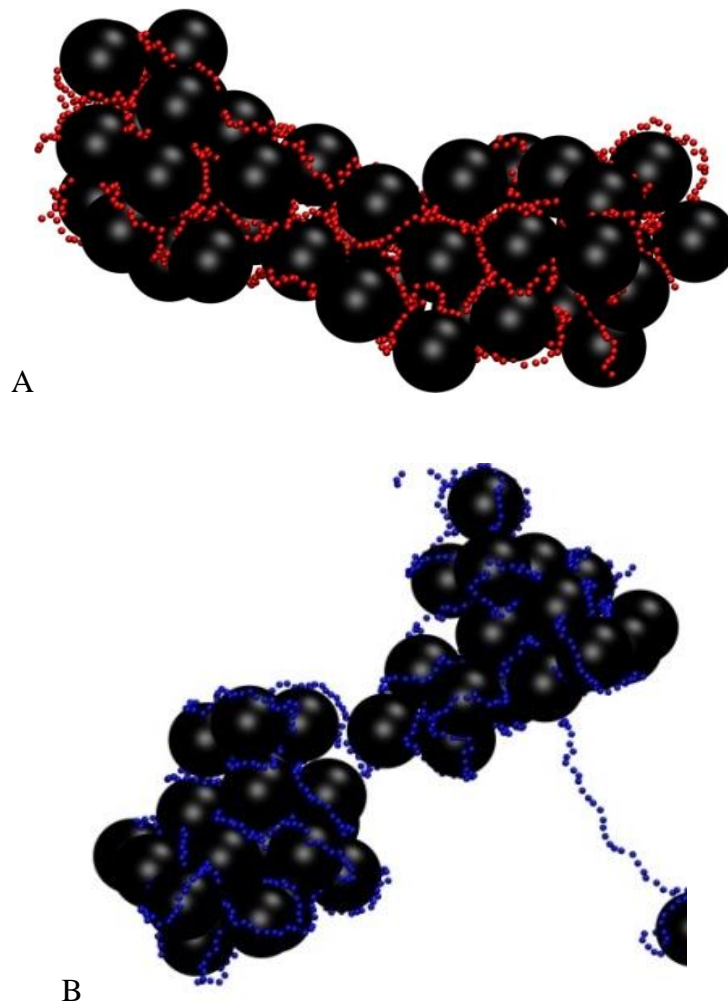
**Figure 3.17:** Snapshots from the 4.0μs BD simulation of G4 dendrimer (black beads) and (a) ssDNA (red beads) as well as (b) dsDNA (blue beads).

Figure 3.18 shows that the values of the toroidal parameter ($\tau \approx 0.22$) for complexes formed of ssDNA and G4 is greater than the values of the toroidal parameter ($\tau \approx 0.16$) for complexes of dsDNA and G4 which indicates that the

47

ssDNA trends to form toroidal structure with G4 dendrimer. So the dsDNA creates disordered morphologies with G4 dendrimer, unlike the structures formed of ssDNA which have morphologies similar to toroid structure.
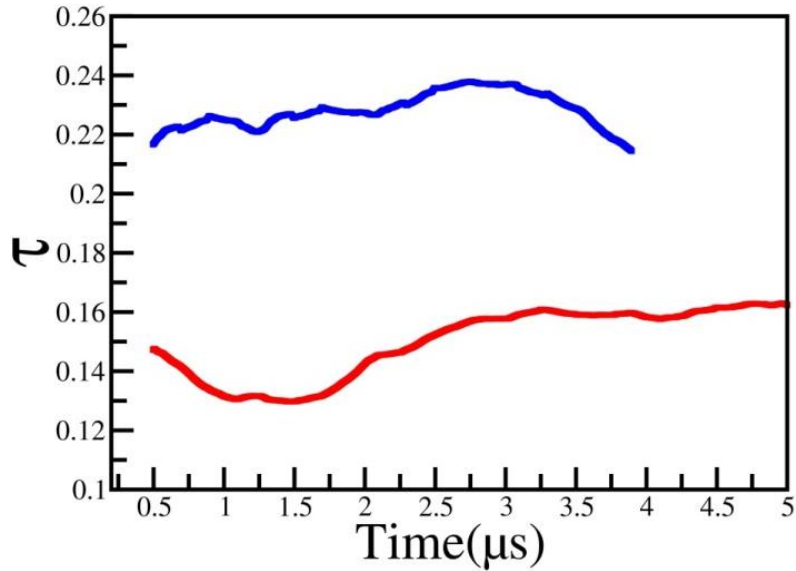
Figure 3.18: The toroidal parameter as a function of time for ssDNA-G4 complex (blue) and dsDNA-G4 (red).

We studied the locations of DNA or dendrimer beads in the aggregates by finding the radial distribution function $g(r)$. Which defines the probability of finding a particle at a distance r from another tagged particle. It can describe the average structure of a molecular system and shows if the structure is ordered or not.

The radial distribution function of pairs of dendrimers in systems composed of 100 spheres of G2 or 43 spheres of G4 with 1362 or 1330ssDNA beads respectively is shown in Figure 3.19 At short distances; less than the dendrimer diameter (29 Å for G2 and 45 Å for G4) $g(r)$ is zero. This is because of the strong repulsive forces as discussed before (equation 2.9). For G2, the first peak is at ≈ 31.5 Å , which means that at this distance there is a high probability

to find two dendrimers at this separation. This separation is very close to the diameter of G2 dendrimer (29 Å) which confirm the compaction with DNA. In G4-ssDNA system the first peak occurs at $r \approx 50$ Å which is also comparable to the diameter of G4 (=45 Å). This indicates that the dendrimer beads are close to each other and compact to form an order structure for both G2 and G4.
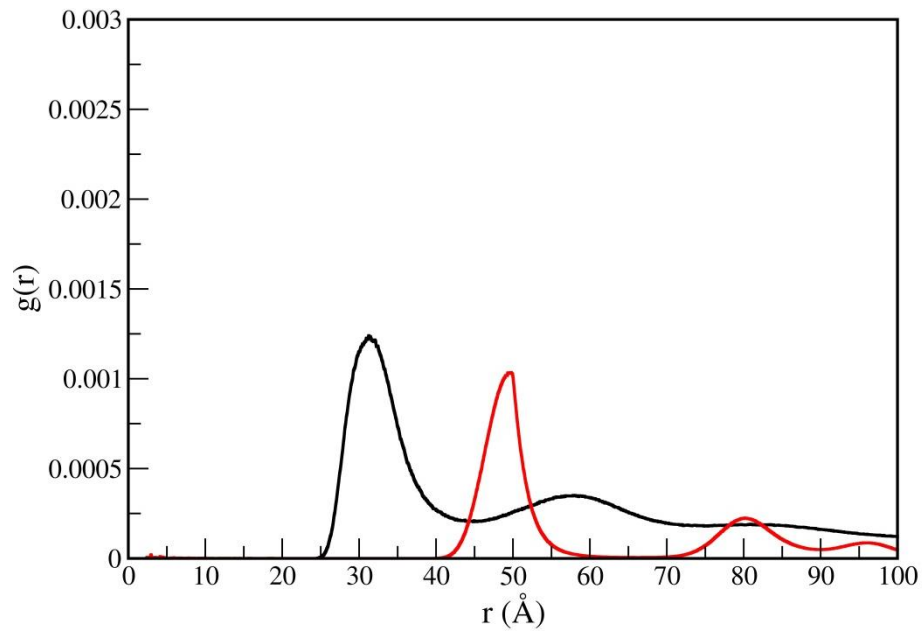
Figure 3.19: g(r) of dendrimer beads for G2-ssDNA aggregate (black) and G4-ssDNA aggregate (red).

We find the radial distribution of dendrimer-DNA in G2-ssDNA and G4-ssDNA aggregates. Figure 3.20 illustrates that ssDNA beads are most likely to be at distance of 17.5 Å, near to the sum of dendrimer radius and DNA bead radius (14.5+2=16.5 Å). This is because of the strong electrostatic forces which enable ssDNA to wrap around dendrimers to form complexes.
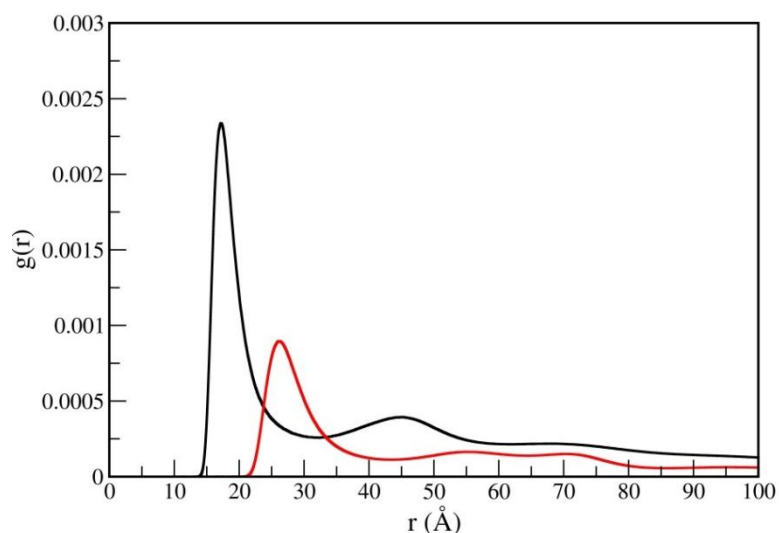
Figure 3.20: g(r) of dendrimer-ssDNA beads for G2(black) and G4(red).

Figure 3.21 shows the distribution function of dendrimers of G4-ssDNA and G4-dsDNA aggregates. g (r) of G4-dsDNA peaked at distance less than G4-ssDNA, so this lead us to conclude that the dsDNA is wrapping more tightly than the ssDNA to form more compact aggregate of dsDNA with G4 dendrimer. The appearance of more than one peak means that the structure of both G4-ssDNA and G4-dsDNA is ordered.
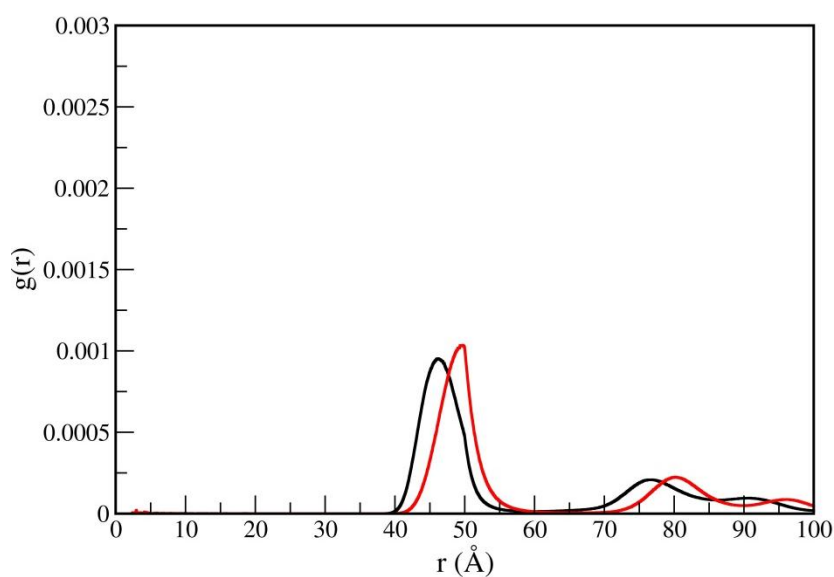
Figure 3.21: g(r) of dendrimer-dednrimer distance of G4-ssDNA aggregate (red) and G4-dsDNA aggregate (black).

50

3.3.　The Effect of DNA Stiffness and Chain Length.

As the DNA chain is represented by bead-spring model, its behavior in the G2-dsDNA complex is influenced by the stiffness or the resistance of the DNA chain to deformation. The stiffness depends on the spring-constant (K) which is measured in units of kcal/mol.Å^2. In this section, we studied the effect of the spring-constant on the toroidal parameter of complexes formed of 10 spheres of G2 dendrimer and 136 beads of dsDNA. We deduced from Figure 3.22 the toroidal parameter versus time for G2-dsDNA aggregates at different DNA stiffness, represented by spring constants, K=0.06 kcal/mol.Å^2, K=0.6 kcal/mol.Å^2, K=2.6 kcal/mol.Å^2.
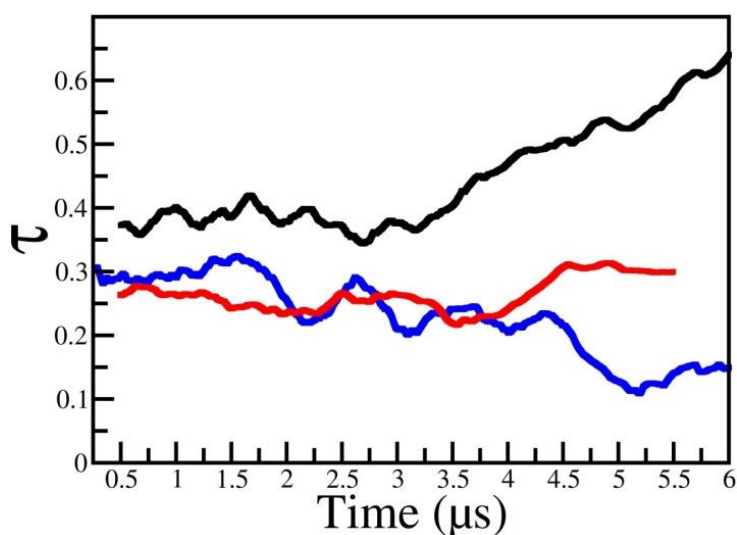
Figure 3.22: The toroidal parameter versus time for G2-dsDNA aggregates (each has10 dendrimer spheres and 136 dsDNA beads). Black: K=0.06 kcal/mol.Å^2. Red: K=0.6 kcal/mol.Å^2. Blue: K=2.6 kcal/mol.Å^2.

The soft DNA chain (K=0.06 kcal/mol.Å^2) has the largest toroidal parameter ($\sim$0.6) so the dsDNA-G2 complex has a disorderd structure. In this case the DNA can easily move and wrap around the dendrimers to form toroidal aggregates. Whereas, the DNA of spring constant of 0.6 kcal/mol.Å^2 has the same value of the toroidal parameter of the stiff DNA (K=2.6 kcal/mol.Å^2) at the first

four microseconds but then the stiff DNA trends to have rod-like structure with toroidal parameter of 0.1, since it cannot move and wrap easily to form toroidal structures.

We carried BD simulations for system contains two different chain lengths of dsDNA (681 beads and 1362 beads) with 50 and 100 spheres of G2 dendrimer respectively, The numbers of DNA and dendrimers are chosen to match their experimental ratio[69]. The values of toroidal parameter τ shown in Figure 3.23 reveal that the short length (681bp) has toroidal parameter larger than the long chain (1362bp) which means that the short DNA form toroidal-like structure comparing to the long one. The toroidal parameter for the aggregate with the short length ($\tau \approx 0.3$) is larger than the toroidal parameter for the aggregate with the long length chain ($\tau \approx 0.1$) that is because the charge of the long length is larger than that of the short one, which makes the dsDNA beads repel each other to form a rod-like structure. Whereas the electrostatic attraction between the short dsDNA and dendrimers is larger than the repulsion between the dsDNA beads themselves.
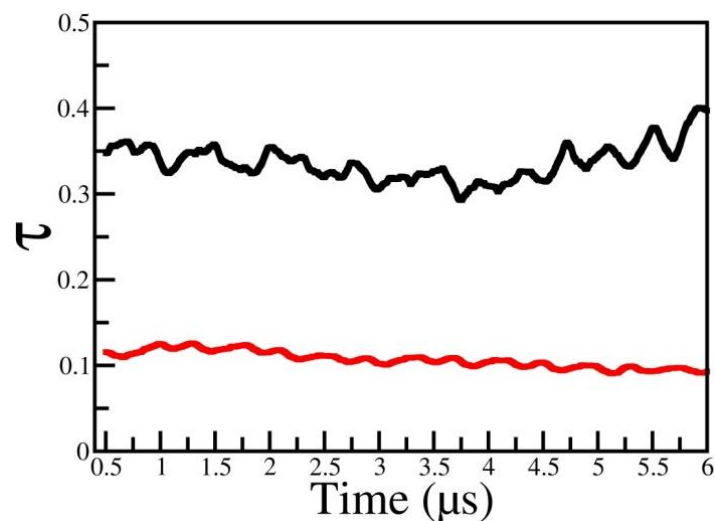
Figure 3.23: Toroidal parameter versus time for aggregate composed of 1362 dsDNA beads with 100 dendrimers (red), and black represents a system of 50 dendrimers with 681 dsDNA beads.

52

Chapter 4: CONCLUSIONS

It is seen that the variation of dendrimer generation affects the degree of absorption of DNA beads on dendrimer surface. Because of their high curvature, lower curvature and higher charge, G4 and G6 dendrimers condense DNA more than lower generations (G2 and G3) at low salt concentration. The degree of absorption of DNA is increased by increasing dendrimer generation for complexes composed of G2, G3, G4, and G6 with ssDNA or dsDNA. Because of its higher total negative charge, ssDNA adsorbed more than dsDNA on dendrimer surface. Increasing salt concentration screens the electrostatic interactions between DNA and dendrimer so reduces the degree of absorption of DNA on dendrimer surface.

The wrapping of DNA around dendrimer is affected by salt concentration. In particularly, increasing salt concentration will increase the screening effects of the ions in the solvent which in turn reduce the electrostatic forces between DNA and dendrimer. The presence of ions affects also on the DNA structure, it will be more straight at high salt concentrations. In contrast to the low salt concentration where DNA is able to wrap according to the dendrimer generation, it wraps less than one turn for G2 and more than one for G4 and G6. Furthermore, the structure of the aggregates formed by three dendrimers and dsDNA are strongly overcharged by the adsorbed dsDNA beads and the degree of overcharging depends on the length of DNA. The increase in the length of the dsDNA leads to increase of linkers between dendrimers. The overcharging degree in complexes of ssDNA is not strong as dsDNA complexes. The morphologies of the DNA aggregates depend on the characteristic of the DNA; length, charge, and stiffness. Our study shows that the dsDNA can form rod-like structure with G2 dendrimer,

whereas ssDNA can form a toroidal structure with G4. The ssDNA did not give a rod-like structure but it gives an ordered structure with G2 dendrimer like the aggregates formed between G4 and dsDNA. The aggregates composed of G2 dendrimer and dsDNA of lengths of 681bp trend to have toroidal morphology whereas the morphology of G2 dendrimer and 1362 bp seems to be as rod-like structure. The flexible dsDNA can form toroidal morphologies with G2 dendrimers while the aggregates of G2 dendrimers and the stiff dsDNA have rod-like structure.

REFERENCES

1.   K. Qamhieh, T. Nylander, C. F. Black, G. S. Attard, R. S. Dias and M.-L. Ainalem, Physical Chemistry Chemical Physics **16** (26), 13112-13122 (2014).
2.   J. D. Watson and F. H. Crick, JAMA **269** (15), 1967-1969 (1993).
3.   M.-L. Ainalem and T. Nylander, Soft Matter **7** (10), 4577-4594 (2011).
4.   J. D. Watson and F. H. Crick, presented at the Cold Spring Harbor symposia on quantitative biology, 1953 (unpublished).
5.   M. Kanehisa and S. Goto, Nucleic acids research **28** (1), 27-30 (2000).
6.   H. Schiessel, Journal of Physics: Condensed Matter **15** (19), R699 (2003).
7.   R. D. Kornberg, Annual review of biochemistry **46** (1), 931-954 (1977).
8.   J. McGhee and G. Felsenfeld, Annual review of biochemistry **49** (1), 1115-1156 (1980).
9.   J. Workman and R. Kingston, Annual review of biochemistry **67** (1), 545-579 (1998).
10.   Y.-q. Ma, Chemical Society Reviews **42** (2), 705-727 (2013).
11.   A. Hamosh, A. F. Scott, J. S. Amberger, C. A. Bocchini and V. A. McKusick, Nucleic acids research **33** (suppl_1), D514-D517 (2005).
12.   E. Giblett, J. Anderson, F. Cohen, B. Pollara and H. Meuwissen, The Lancet **300** (7786), 1067-1069 (1972).
13.   D. B. Kohn, K. I. Weinberg, J. A. Nolta, L. N. Heiss, C. Lenarsky, G. M. Crooks, M. E. Hanley, G. Annett, J. S. Brooks and A. El-Khoureiy, Nature medicine **1** (10), 1017-1023 (1995).
14.   A. Aiuti, F. Cattaneo, S. Galimberti, U. Benninghoff, B. Cassani, L. Callegaro, S. Scaramuzza, G. Andolfi, M. Mirolo and I. Brigida, New England Journal of Medicine **360** (5), 447-458 (2009).
15.   J. Hardy and D. J. Selkoe, science **297** (5580), 353-356 (2002).
16.   A. Sayyed-Ahmad, K.-J. Cho, J. F. Hancock and A. A. Gorfe, The Journal of Physical Chemistry B **120** (33), 8547-8556 (2016).
17.   P. Prakash, A. Sayyed-Ahmad, K.-J. Cho, D. M. Dolino, W. Chen, H. Li, B. J. Grant, J. F. Hancock and A. A. Gorfe, Scientific reports **7** (2017).
18.   A. Sayyed-Ahmad, H. Khandelia and Y. N. Kaznessis, Molecular simulation **35** (10-11), 986-997 (2009).
19.   A. Sayyed-Ahmad, L. M. Lichtenberger and A. A. Gorfe, Langmuir **26** (16), 13407-13414 (2010).
20.   A. Sayyed-Ahmad, K. Volzing, V. Vivcharuk and S. Poonam, (2014).
21.   S. M. Moghimi, A. C. Hunter and J. C. Murray, The FASEB journal **19** (3), 311-330 (2005).
22.   J. Khandare, M. Calderón, N. M. Dagia and R. Haag, Chemical Society Reviews **41** (7), 2824-2848 (2012).
23.   M. A. Mintzer and M. W. Grinstaff, Chemical Society Reviews **40** (1), 173-190 (2011).
24.   T. Friedmann and R. Roblin, Science **175** (4025), 949-955 (1972).
25.   R. I. Mahato and S. W. Kim, *Pharmaceutical Perspectives of Nucleic Acid-Based Therapy*. (CRC Press, 2003).
26.   T. Niidome and L. Huang, Gene therapy **9** (24), 1647-1652 (2002).
27.   J.-M. Escoffre, J. Teissié and M.-P. Rols, The Journal of membrane biology **236** (1), 61-74 (2010).
28.   S. Li and L. Huang, Gene therapy **7** (1), 31-34 (2000).

29.   S. Svenson and D. A. Tomalia, Advanced drug delivery reviews **64**, 102-115 (2012).
30.   A. K. Patri, J. F. Kukowska-Latallo and J. R. Baker, Advanced drug delivery reviews **57** (15), 2203-2214 (2005).
31.   U. Boas and P. M. Heegaard, Chemical Society Reviews **33** (1), 43-63 (2004).
32.   B. K. Nanjwade, H. M. Bechra, G. K. Derkar, F. Manvi and V. K. Nanjwade, European Journal of Pharmaceutical Sciences **38** (3), 185-196 (2009).
33.   E. Abbasi, S. F. Aval, A. Akbarzadeh, M. Milani, H. T. Nasrabadi, S. W. Joo, Y. Hanifehpour, K. Nejati-Koshki and R. Pashaei-Asl, Nanoscale Research Letters **9** (1), 247 (2014).
34.   S. G. Sampathkumar and K. J. Yarema, Nanotechnologies for the Life Sciences (2007).
35.   D. A. Tomalia, Scientific American **272** (5), 62-66 (1995).
36.   J. P. Bharti, S. Prajapati, M. K. Jaiswal and R. D. Yadav.
37.   D. A. Tomalia, H. Baker, J. Dewald, M. Hall, G. Kallos, S. Martin, J. Roeck, J. Ryder and P. Smith, Polymer Journal **17** (1), 117-132 (1985).
38.   B. Klajnert½ and M. Bryszewska, (2001).
39.   G. R. Newkome, Z. Yao, G. R. Baker and V. K. Gupta, The Journal of Organic Chemistry **50** (11), 2003-2004 (1985).
40.   G. Newkome, Z. Yao, G. Baker and V. Gupta, presented at the ABSTRACTS OF PAPERS OF THE AMERICAN CHEMICAL SOCIETY, 1985 (unpublished).
41.   D. A. Tomalia, Aldrichimica Acta **37** (2), 39-57 (2004).
42.   A. Bosman, H. Janssen and E. Meijer, Chemical reviews **99** (7), 1665-1688 (1999).
43.   E. R. Gillies and J. M. Frechet, Drug discovery today **10** (1), 35-43 (2005).
44.   Y. Kim and S. C. Zimmerman, Current opinion in chemical biology **2** (6), 733-742 (1998).
45.   P. K. Maiti and B. Bagchi, Nano letters **6** (11), 2478-2485 (2006).
46.   C. J. Hawker and J. M. Frechet, Journal of the American Chemical Society **112** (21), 7638-7647 (1990).
47.   S. Pushkar, A. Philip, K. Pathak and D. Pathak, Indian Journal of Pharmaceutical Education and Research **40** (3), 153 (2006).
48.   M. Fischer, D. Appelhans, S. Schwarz, B. Klajnert, M. Bryszewska, B. Voit and M. Rogers, Biomacromolecules **11** (5), 1314-1325 (2010).
49.   E. R. Gillies, E. Dy, J. M. Fréchet and F. C. Szoka, Molecular pharmaceutics **2** (2), 129-138 (2005).
50.   J. Lim, G. M. Pavan, O. Annunziata and E. E. Simanek, Journal of the American Chemical Society **134** (4), 1942-1945 (2012).
51.   K. Ciepluch, N. Katir, A. El Kadib, A. Felczak, K. Zawadzka, M. Weber, B. Klajnert, K. Lisowska, A.-M. Caminade and M. Bousmina, Molecular pharmaceutics **9** (3), 448-457 (2012).
52.   T. P. Thomas, A. K. Patri, A. Myc, M. T. Myaing, J. Y. Ye, T. B. Norris and J. R. Baker, Biomacromolecules **5** (6), 2269-2274 (2004).
53.   L.-Y. Jiang, B. Lv and Y. Luo, Biomaterials **34** (11), 2665-2673 (2013).
54.   R. C. Hedden and B. J. Bauer, Macromolecules **36** (6), 1829-1835 (2003).
55.   P.-G. de Gennes and H. Hervet, Journal de Physique Lettres **44** (9), 351-360 (1983).
56.   A. M. Naylor, W. A. Goddard III, G. E. Kiefer and D. A. Tomalia, Journal of the American Chemical Society **111** (6), 2339-2341 (1989).
57.   F. Zeng and S. C. Zimmerman, Chemical Reviews **97** (5), 1681-1712 (1997).
58.   J. P. Bharti, S. Prajapati, M. K. Jaiswal and R. D. Yadav, International Journal of Pharmaceutical Sciences and Research **2** (8), 1947-1960 (2011).

59.   P. Hodge, Nature **362** (6415), 18-19 (1993).
60.   S. M. Grayson and J. M. Frechet, Chemical Reviews **101** (12), 3819-3868 (2001).
61.   N. Martinho, H. Florindo, L. Silva, S. Brocchini, M. Zloh and T. Barata, Molecules **19** (12), 20424-20467 (2014).
62.   M. L. Mansfield and L. I. Klushin, Macromolecules **26** (16), 4262-4268 (1993).
63.   M. K. Bhalgat and J. C. Roberts, European polymer journal **36** (3), 647-651 (2000).
64.   R. Esfand and D. A. Tomalia, Drug discovery today **6** (8), 427-436 (2001).
65.   M. X. Tang, C. T. Redemann and F. C. Szoka, Bioconjugate chemistry **7** (6), 703-714 (1996).
66.   A. K. Patri, I. J. Majoros and J. R. Baker, Current opinion in chemical biology **6** (4), 466-471 (2002).
67.   I. J. Majoros, A. Myc, T. Thomas, C. B. Mehta and J. R. Baker, Biomacromolecules **7** (2), 572-579 (2006).
68.   I. J. Majoros, T. P. Thomas, C. B. Mehta and J. R. Baker, Journal of medicinal chemistry **48** (19), 5892-5899 (2005).
69.   K. Barbara and B. Maria, Acta biochimica polonica **48** (1), 199-208 (2001).
70.   M. Fleharty, 2010.
71.   N. Kopidakis, W. Mitchell, J. Bozell, J. Piris, D. Ginley, G. Rumbles and S. Shaheen, 2005.
72.   K. Qamhieh, T. Nylander and M.-L. Ainalem, Biomacromolecules **10** (7), 1720-1726 (2009).
73.   M. Mills, B. Orr, M. M. B. Holl and I. Andricioaei, Biophysical journal **98** (5), 834-842 (2010).
74.   J. F. Kukowska-Latallo, A. U. Bielinska, J. Johnson, R. Spindler, D. A. Tomalia and J. R. Baker, Proceedings of the National Academy of Sciences **93** (10), 4897-4902 (1996).
75.   M. Ottaviani, B. Sacchi, N. Turro, W. Chen, S. Jockusch and D. Tomalia, Macromolecules **32** (7), 2275-2282 (1999).
76.   W.-R. Chen, L. Porcar, Y. Liu, P. D. Butler and L. J. Magid, Macromolecules **40** (16), 5887-5898 (2007).
77.   S. Rosenfeldt, N. Dingenouts, M. Ballauff, P. Lindner, C. Likos, N. Werner and F. Vögtle, Macromolecular Chemistry and Physics **203** (13), 1995-2004 (2002).
78.   S. Seelenmeyer and M. Ballauff, Langmuir **16** (9), 4094-4099 (2000).
79.   C.-Y. Chen, C.-J. Su, S.-F. Peng, H.-L. Chen and H.-W. Sung, Soft Matter **7** (1), 61-63 (2011).
80.   Y. Cheng, Q. Wu, Y. Li, J. Hu and T. Xu, The Journal of Physical Chemistry B **113** (24), 8339-8346 (2009).
81.   S. Yu, M.-H. Li, S. K. Choi, J. R. Baker and R. G. Larson, Molecules **18** (9), 10707-10720 (2013).
82.   M.-L. Örberg, K. Schillén and T. Nylander, Biomacromolecules **8** (5), 1557-1563 (2007).
83.   E. Froehlich, J. Mandeville, C. Weinert, L. Kreplak and H. Tajmir-Riahi, Biomacromolecules **12** (2), 511-517 (2010).
84.   P. J. Bond, J. Holyoake, A. Ivetac, S. Khalid and M. S. Sansom, Journal of structural biology **157** (3), 593-605 (2007).
85.   H. Lee and R. G. Larson, The Journal of Physical Chemistry B **112** (26), 7778-7784 (2008).
86.   P. Welch and M. Muthukumar, Macromolecules **33** (16), 6159-6167 (2000).
87.   S. V. Lyulin, A. A. Darinskii and A. V. Lyulin, Macromolecules **38** (9), 3990-3998 (2005).

88.   S. V. Larin, A. A. Darinskii, A. V. Lyulin and S. V. Lyulin, The Journal of Physical Chemistry B **114** (8), 2910-2919 (2010).
89.   S. Larin, S. Lyulin, A. Lyulin and A. Darinskii, Polymer Science Series A **51** (4), 459-468 (2009).
90.   T. Terao and T. Nakayama, Macromolecules **37** (12), 4686-4694 (2004).
91.   G. M. Pavan, M. A. Mintzer, E. E. Simanek, O. M. Merkel, T. Kissel and A. Danani, Biomacromolecules **11** (3), 721-730 (2010).
92.   S. V. Lyulin, I. Vattulainen and A. A. Gurtovenko, Macromolecules **41** (13), 4961-4968 (2008).
93.   Y.-q. Ma, Soft Matter **7** (2), 500-505 (2011).
94.   K. Qamhieh and A. A. Khaleel, Colloids and Surfaces A: Physicochemical and Engineering Aspects **442**, 191-198 (2014).
95.   S. Yu and R. G. Larson, Soft matter **10** (29), 5325-5336 (2014).
96.   M.-L. Ainalem, A. M. Carnerup, J. Janiak, V. Alfredsson, T. Nylander and K. Schillén, Soft Matter **5** (11), 2310-2320 (2009).
97.   K. Qamhieh, T. Nylander, C. F. Black, G. S. Attard, R. S. Dias and M.-L. Ainalem, Physical Chemistry Chemical Physics (2014).
98.   A. Einstein, *Investigations on the Theory of the Brownian Movement*. (Courier Corporation, 1956).
99.   J. Klafter, M. F. Shlesinger and G. Zumofen, Physics today **49** (2), 33-39 (1996).
100.   M. Długosz, P. Zieliński and J. Trylska, Journal of computational chemistry **32** (12), 2734-2744 (2011).
101.   D. L. Ermak and J. McCammon, The Journal of chemical physics **69**, 1352 (1978).
102.   A. Arkhipov, P. L. Freddolino and K. Schulten, Structure **14** (12), 1767-1777 (2006).
103.   G. D. R. o. Echenique, R. R. g. Schmidt, J. J. Freire, J. G. H. Cifre and J. G. a. d. l. Torre, Journal of the American Chemical Society **131** (24), 8548-8556 (2009).
104.   G. K. Fraenkel, The Journal of Chemical Physics **20** (4), 642-647 (1952).
105.   P. E. Rouse Jr, The Journal of Chemical Physics **21** (7), 1272-1280 (1953).
106.   H. R. Warner Jr, Industrial & Engineering Chemistry Fundamentals **11** (3), 379-387 (1972).
107.   F. Diaz and J. García de La Torre, The Journal of chemical physics **88** (12), 7698-7705 (1988).
108.   R. Pamies, J. Cifre, D. La Torre and J. García, Journal of Polymer Science Part B: Polymer Physics **45** (1), 1-9 (2007).
109.   A. Sayyed–Ahmad, K. Tuncay and P. J. Ortoleva, Journal of computational chemistry **25** (8), 1068-1074 (2004).
110.   D. L. Ermak and J. McCammon, The Journal of chemical physics **69** (4), 1352-1360 (1978).
111.   A. Iniesta and J. Garcia de la Torre, The Journal of Chemical Physics **92** (3), 2015-2018 (1990).
112.   M. Jonsson and P. Linse, The Journal of Chemical Physics **115** (7), 3406-3418 (2001).
113.   M. Jonsson and P. Linse, The Journal of Chemical Physics **115** (23), 10975-10985 (2001).
114.   T. Sakaue, K. Yoshikawa, S. H. Yoshimura and K. Takeyasu, Physical review letters **87** (7), 078105 (2001).
115.   Q. Cao, C. Zuo, Y. Ma, L. Li and Z. Zhang, Soft Matter **7** (2), 506-514 (2011).
116.   D. G. Angelescu, R. Bruinsma and P. Linse, Physical Review E **73** (4), 041921 (2006).

117.   S. C. Nunes, M. Skepö and A. A. Pais, Journal of computational chemistry **36** (21), 1579-1586 (2015).
118.   M. R. Wright, *An introduction to aqueous electrolyte solutions*. (John Wiley & Sons, 2007).
119.   B. Nandy and P. K. Maiti, The Journal of Physical Chemistry B **115** (2), 217-230 (2010).
120.   K. Luger, A. W. Mäder, R. K. Richmond, D. F. Sargent and T. J. Richmond, Nature **389** (6648), 251-260 (1997).

APPENDICES

Writing the BD-BOX input files

Two input files are required to perform the BD simulations. one is the structure file which contains 11 columns: "sub", name of the particle, particle id, x coordinate, y coordinate, z coordinate, hydrodynamic radius, charge, the double of the radius of gyration, the Lennard-Jones constant and the last column for the mass of the particle. The second one is the parameter file which containing the all the parameters of the simulation. Below is the a fortran script that used to generate the input files for our BD simulations.

```
c Generation 2
 implicit none
        integer i, f(62),j ,k ,flag ,skip ,ff(62)
        double precision mass, radius,r(62),m(62),c,d,dd
        double precision x(55520),y(55520),z(55520),n
        double precision u(55520),v(55520),q(55520),rr(55520)
 double precision dna_radius, dend_radius, term_radius
        double precision deltatheta,theta,dendcharge
 character*4 p,p1,cc,gg
        integer dnanum,dendnum,count,e
        double precision l,volume,volume_fraction
        double precision x0,bond_length
        double precision xmin,ymin,zmin,xmax,ymax,zmax
        xmin=-150.367
        ymin=-150.899
        zmin=-144.9669
        xmax=149.6329956
```

```fortran
      ymax=149.10099

      zmax=145.166

      l=330.92

      volume=l**3

      OPEN (UNIT=11, FILE = 'gen-2-dend.str')

      OPEN (UNIT=12, FILE = 'gen-2-dend.prm')

      x0=((volume*volume_fraction)**(1.0/3.0))/4.0

      dendnum=1

 dnanum=19

 dna_radius=2.0

      dend_radius=14.5

      bond_length=4.0

       deltatheta=19.31

      dendcharge=16
c ***************** The initial position of DNA *********

      x(1)=-100.0

      y(1)=0.0

      z(1)=10.0

 do j=2,dnanum
c 100.0 is the radius of the helix
c  25.0  is  the  reciprocal  of  the  frequency(1/N);  N=radius  of  the
helix*2*pi/bond_length

      x(j)=150.0*cos(2*3.14*j/37.5)

      y(j)=150.0*sin(2*3.14*j/37.5)

      z(j)=2*j*bond_length/37.5

      enddo
c **************The initial position of dendrimer***********
 u(1)=0.0

 v(1)=0.0

      q(1)=0.0
```

```fortran
      u(2)=(xmin/10.0)+30.011

      v(2)=(ymin/10.0)+3.011

      q(2)=(zmin/10.0)+2.56

      u(3)=(xmin/4.0)

      v(3)=(ymin/2.0)

      q(3)=-1*(zmin/2.0)

 do k=1,dendnum

      write(11,28) "sub","dend",k,u(k),v(k),q(k),

+     dend_radius,dendcharge,2*dend_radius,0.178,1.0

      enddo

      do i=1,dnanum

 write(11,28) "sub","DNA",i+dendnum,x(i),y(i),z(i),

+     dna_radius,-2.0,2*dna_radius,0.178,1.0

      enddo

28     format(A10,A12,I5,F10.3,F11.3,F10.3,F10.3,F8.1,F10.1,

+ F4.1,F10.1)

 do i=1,dnanum-1

      write(11,29) "bond",i+dendnum,i+1+dendnum,2*dna_radius,

+ 1000000.0,0.6

 enddo

29     format (A10,I5,I5,F10.3,F13.3,F10.3)

 do i=1,dnanum-2

      write(11,30) "angle","angle",i,i+1,i+2,167.0,0.005

      enddo

30     format (A10,A10,I5,I5,I5,F10.3,F13.3)

Ccccccccccccc the parameter file


      write(12,*) "dt 0.1"

      write(12,*) "T 298.0"
```

```
write(12,*) "visc 0.0235"
        write(12,*) "vfactor 14.4"
        write(12,*) "bdsteps 3000000000"
        write(12,*) "save_dcd_freq 500"
        write(12,*) "save_rst_freq 500"
        write(12,*) "save_enr_freq 500"
        write(12,*) "save_xyz_freq 500"
        write(12,*) "xyz_filename gen-2-dend.xyz"
        write(12,*) "dcd_filename gen-2-dend.dcd"
        write(12,*) "enr_filename gen-2-dend.enr"
        write(12,*) "str_filename gen-2-dend.str"
        write(12,*) "out_filename gen-2-dend.out"
        write(12,*) "pqr_filename gen-2-dend.pqr"
        write(12,*) "rst_filename gen-2-dend.rst"
        write(12,*) "alpha_lj 4.0"
        write(12,*) "gamma_c 331.842"
        write(12,*) "bond_c_scale 0.0"
        write(12,*) "cutoff_c 50.0"
        write(12,*) "kappa_c 0.033"
        write(12,*) "check_overlap no"
        write(12,*) "lj_6_term yes"
        write(12,*) "elec yes"
        write(12,*) "move_attempts 1000000"
        write(12,*) "cutoff_lj -1"
        write(12,*) "bond_lj_scale 0.0"
        write(12,*) "algorithm ermak_const"
        write(12,*) "rand_seed 997"
        write(12,*) "hydro none"
        write(12,*) "epsilon_c 55"
```

```fortran
      write(12,*) "nb_list brute"
      write(12,*) "xbox",330.92
      write(12,*) "ybox",330.92
      write(12,*) "zbox",330.92
      write(12,*) "bc pbc"
 end
```

Computing the distance between the DNA and dendrimer

Below is the fortran script used to calculate the distance between the center of mass of DNA chain and center of mass of dendrimer.

```fortran
 implicit none
 character*4 junk
      double precision junck,charge,radius,cratio
      integer i,jnk,dendnum,dnanum,j,count,Natoms,Nframes
      integer k,ss,count1,dnacom,s,kk,m,flag(22)
      double precision dna_radius,dend_radius,dend_charge
      double precision dna_charge,comp_charge(199)
      double precision traj(60000,20,3),x(60000,20,3)
      double precision sum1(60000),sum2(60000),sum3(60000)
      double precision xd(60000),yd(60000),zd(60000)
      double precision r(60000),xcom(60000),ycom(60000)
      double precision zcom(60000)
      double precision ravg,sigma,diff,sum
open(unit=13, file='gen-2-dend.xyz')
      open(unit=14, file='dis-2-10-ds.out')
      dnanum=19
 dendnum=1
      Natoms=20
```

```
      nframes= 50000
            dna_charge=-2.0
            dend_charge=16.0
            dna_radius= 2.0
            dend_radius=14.5
c do loop on the number of dendrimers, each dend how many dna beads turn
around it!
 do i=1,nframes
             read(13,*)
             read(13,*)
             do j=1,natoms
 read(13,*) junk,traj(i,j,1),traj(i,j,2),traj(i,j,3)
 enddo
 enddo
            close(13)
 sum=0.0
            do i=1,nframes
             sum1(i)=0.0
             sum2(i)=0.0
             sum3(i)=0.0
             do k=dendnum+1,natoms
             sum1(i)=sum1(i)+traj(i,k,1)
             sum2(i)=sum2(i)+traj(i,k,2)
             sum3(i)=sum3(i)+traj(i,k,3)
 enddo
            xcom(i)=sum1(i)/dnanum
            ycom(i)=sum2(i)/dnanum
            zcom(i)=sum3(i)/dnanum
 xd(i)=xcom(i)-traj(i,1,1)
 yd(i)=ycom(i)-traj(i,1,2)
```

65

```fortran
      zd(i)=zcom(i)-traj(i,1,3)

      r(i)=sqrt(xd(i)**2+yd(i)**2+zd(i)**2)

      write(14,*) i*100/1d6,r(i)

            sum=sum+r(i)

      enddo

      end
```

      zd(i)=zcom(i)-traj(i,1,3)

Computing the curvature parameter

Below is the fortran script used to calculate the curvature parameter that was discussed in chapter 2 equation: 2.12.

```fortran
 implicit none
        character*4 junk
        double precision junck,charge,radius,cratio
        integer i,jnk,dendnum,dnanum,j,count,Natoms,Nframes
        integer k,ss,count1,dnacom,s,kk,m,flag(22)
        double precision dna_radius,dend_radius,dend_charge
        double precision dna_charge,comp_charge(199)
        double precision traj(20,3),y,dnacomp(20,3),x(22,22,3)
        double precision sum1,sum2,sum3,eta,xx(20,3),x1(22,22,3)
 open(unit=13, file='gen-2-dend.xyz')
        open(unit=14, file='gen-2-curv.out')
        dnanum=19
 dendnum=1
         Natoms=20
 dna_charge=-2.0
        dend_charge=16.0
        dna_radius=2.0
        dend_radius=14.5
c do loop on the num of dend, each dend how many dna beads turn around it!
        do j=1,natoms
 read(13,*) junk,traj(j,1),traj(j,2),traj(j,3)
 enddo
 close(13)
```

```
dnacom=0
do k=dendnum+1,Natoms
        y=sqrt((traj(1,1)-traj(k,1))**2+ (traj(1,2)-
+ traj(k,2))**2+(traj(1,3)-traj(k,3))**2)
if(abs(y-(dend_radius+dna_radius))<7.0) then
        kk=k
        dnacomp(kk,1)=traj(k,1)
        dnacomp(kk,2)=traj(k,2)
        dnacomp(kk,3)=traj(k,3)
        dnacom=dnacom+1
        endif
        enddo
do i=dendnum+1,dnacom-1
        x(i,i+1,1)=dnacomp(i+1,1)-dnacomp(i,1)
        x(i,i+1,2)=dnacomp(i+1,2)-dnacomp(i,2)
        x(i,i+1,3)=dnacomp(i+1,3)-dnacomp(i,3)

        x1(i,i+1,1)=x(i,i+1,1)/sqrt(x(i,i+1,1)**2+
+ x(i,i+1,2)**2+x(i,i+1,3)**2)
        x1(i,i+1,1)=x(i,i+1,2)/sqrt(x(i,i+1,2)**2+
+ x(i,i+1,2)**2+x(i,i+1,3)**2)
        x1(i,i+1,3)=x(i,i+1,3)/sqrt(x(i,i+1,1)**2+
+ x(i,i+1,2)**2+x(i,i+1,3)**2)
        enddo
        sum1=0.0
        sum2=0.0
        sum3=0.0
```

```fortran
      do i=dendnum+1,dnacom-1
 xx(i,1)=x1(i,i+1,2)*x1(i+1,i+2,3)-x1(i,i+1,3)*x1(i+1,i+2,2)
      xx(i,2)=x1(i,i+1,3)*x1(i+1,i+2,1)-x1(i,i+1,1)*x1(i+1,i+2,3)
      xx(i,3)=x1(i,i+1,3)*x1(i+1,i+2,2)-x1(i,i+1,2)*x1(i+1,i+2,1)
c     write(14,*) xx(i,1),xx(i,2),xx(i,3)
      sum1=sum1+xx(i,1)
      sum2=sum2+xx(i,2)
      sum3=sum3+xx(i,3)
      enddo
      eta=sqrt(sum1**2+sum2**2+sum3**2)/19
      write(14,*) eta
      end
```

Computing the toroidal parameter

Below is the fortran script used to calculate the order parameter that was discussed in chapter 2 equation: 2.15.

```fortran
 implicit none
        character*4 junk
        double precision junck,charge,radius,cratio
        integer i,jnk,dendnum,dnanum,j,count,Natoms,Nframes
 integer k,ss,count1,s,kk,m,mm
 double precision dna_radius,dend_radius,dend_charge
 double precision dna_charge
 double precision traj(8000,1462,3),y
 double precision sum1(100000,3),sum2(30000),sum3(30000)
 double precision eta(100000),xx(100000,100,3)
 double precision x2(100000,100,3)
 double precision x(8000,100,100,3),summ(100000)
 double precision etaavg, sigma,sum
 open(unit=13, file='gen-2-new.xyz')
 open(unit=14, file='toroidal-G2-ds.out')
 dnanum=1362
 dendnum=100
 Natoms=1462
 nframes=24151
 dna_charge=-2.0
 dend_charge=16.0
 dna_radius=2.0
 dend_radius=14.5
 do i=1,nframes,100
        read(13,*)
```

```fortran
      read(13,*)
       do j=1,natoms
       read(13,*) junk,traj(i,j,1),traj(i,j,2),traj(i,j,3)
  enddo
      enddo
 close(13)
c      sum=0.0
      do i=1,nframes,100
       do mm=1,3
c                i=nframes
 do k=2,dendnum
      x(i,k-1,k,mm)=traj(i,k,mm)-traj(i,k-1,mm)
 enddo
      enddo
      Summ(i)=0.0
      do mm=1,3
      sum1(i,mm)=0.0
      do k=2,dendnum-1
 xx(i,k,1)=x(i,k-1,k,2)*x(i,k,k+1,3)-x(i,k-1,k,3)*
+ x(i,k,k+1,2)
      xx(i,k,2)=x(i,k-1,k,3)*x(i,k,k+1,1)-x(i,k-1,k,1)*
+ x(i,k,k+1,3)
      xx(i,k,3)=x(i,k-1,k,1)*x(i,k,k+1,2)-x(i,k-1,k,2)*
+ x(i,k,k+1,1)
      x2(i,k,mm)=xx(i,k,mm)/sqrt(xx(i,k,1)**2+
+ xx(i,k,2)**2+xx(i,k,3)**2)
      sum1(i,mm)=sum1(i,mm)+x2(i,k,mm)
      enddo
```

71

```
Summ(i)=Summ(i)+(sum1(i,mm))**2

enddo

eta(i)=Summ(i)**0.5/(dendnum-2)

write(14,*) i*100/1d6,eta(i)

enddo

end
```